

Aus der Klinischen Kooperationseinheit Dermatoonkologie des Deutschen
Krebsforschungszentrums (DKFZ) an der Klinik für Dermatologie, Venerologie
und Allergologie der Medizinischen Fakultät Mannheim
(Direktor: Prof. Dr. med. Jochen Utikal)

HSP90 α induces immunosuppressive myeloid cells in melanoma
via TLR4 signaling

Inauguraldissertation
zur Erlangung des medizinischen Doktorgrades
der
Medizinischen Fakultät Mannheim
der Ruprecht-Karls-Universität
zu
Heidelberg

vorgelegt von
Ihor Arkhypov

aus
Dnipro, Ukraine

Dekan: Prof. Dr. med. Sergij Goerd

Referent: Prof. Dr. Jochen Utikal

To my family

TABLE OF CONTENTS

1 LIST OF ABBREVIATIONS	7
2 SUMMARY	10
3 INTRODUCTION.....	12
3.1 Melanoma	12
3.2 ICI in melanoma	12
3.3 The tumor microenvironment (TME).....	13
3.2.1 MDSC	15
3.2.2 Crosstalk between tumor and myeloid cells by means of extracellular vesicles	18
3.3 Heat-shock protein 90.....	21
3.4 Aim of the thesis.....	24
4 MATERIAL AND METHODS	25
4.1 Material.....	25
4.1.1 Protein expression and purification	25
4.1.2 Cell line	25
4.1.3 Cell culture products	25
4.1.4 Cell culture media	26
4.1.5 Kits	27
4.1.6 Antibodies	28
4.1.7 Primers for mRNA	29
4.1.8 Chemicals and biological reagents.....	29
4.1.9 Solutions	31
4.1.10 Routine laboratory material	32
4.1.11 Laboratory equipment	33
4.1.12 Software for data analysis	35
4.2 Methods	35

4.2.1 Cell culture.....	35
4.2.2 Nucleic acid analysis.....	37
4.2.3 Protein analysis	38
4.2.4 Protein expression and purification	41
4.2.5 Magnetic-activated cell sorting (MACS).....	42
4.2.6 Fluorescence-activated cell sorting (FACS) analysis	43
4.2.7 Inhibition of T cell proliferation assay.....	44
4.2.8 Transwell migration assay	45
4.2.9 Patients.....	45
4.2.10 Statistical analysis.....	46
5 RESULTS.....	47
5.1 Expression and purification of the recombinant (r) HSP90 α	47
5.2 Recombinant HSP90 α triggers TLR4 signaling in human monocytes to induce PD-L1 expression	50
5.3 Recombinant HSP90 α converts human monocytes into suppressive myeloid cells and rescues them from apoptosis via TLR4 signaling	53
5.4 rHSP90 α -treated monocytes acquired immunosuppressive capacity via TLR4- dependent upregulation of PD-L1	57
5.5 Expression of MDSC-related genes in rHSP90 α -stimulated monocytes	59
5.6 TLR4-NF- κ B-dependent upregulation of IDO-1 endows rHSP90 α -treated monocytes with immunosuppressive capacity.....	61
5.7 HSP90 α in plasma of melanoma patients.....	63
6 DISCUSSION	67
6.1 Control of the LPS contamination in the rHSP90 α	67
6.2 Upregulation of PD-L1 in rHSP90 α -treated monocytes is TLR4-NF- κ B-dependent	68
6.3 rHSP90 α modifies monocytes towards the suppressive phenotype with prolonged survival	70
6.4 Human monocytes acquire PD-L1-mediated suppressive capacity against T cells after stimulation with rHSP90 α	71

6.5	72
6.6	73
7 REFERENCES	75
8 CURRICULUM VITAE	87
9 LIST OF OWN PUBLICATIONS DURING THE THESIS WORK.....	88
10 ACKNOWLEDGEMENTS	89

1 LIST OF ABBREVIATIONS

1-D-MT	1-methyl-D-tryptophan
7-AAD	7-aminoactinomycin D
ADP	adenosine diphosphate
Akt	AKT serine/threonine kinase 1
APC	antigen presenting cells
Arg-1	arginase-1
ATP	adenosine triphosphate
ATRA	all-trans retinoic acid
BAX	BCL2 associated X
Bay	Bay 11-7082
BCA	bicinchoninic acid
BCL 2	B-cell lymphoma 2
Bcl-xL	B cell lymphoma-extra large
BRAF	serine/threonine-protein kinase B-raf
CAF	cancer-associated fibroblasts
CCL	C-C motif ligand
CCR	C-C chemokine receptor type
CD	cluster of differentiation
CFSE	carboxyfluorescein succinimidyl ester
COX2	cyclooxygenase-2
CTLA-4	cytotoxic T lymphocyte-associated protein-4
CXCR	CXC chemokine receptor
DC	dendritic cells
DMSO	dimethylsulfoxid
DNA	deoxyribonucleic acid
DPBS	Dulbecco's phosphate-buffered saline
EGFR	epidermal growth factor receptor
eHSP90	extracellular HSP90
ELISA	enzyme-linked immunosorbent assay
ERK	extracellular-signal regulated kinase
EV	extracellular vesicles
FACS	fluorescence-activated cell sorting
FAP	fibroblast activation protein
FasL	Fas ligand
G	granulocyte
GM-CSF	granulocyte-macrophage colony stimulating factor
Grp94	94-kDa glucose-related protein
HHC	hepatocellular carcinoma
HIF	hypoxia inducible factor
HLA-DR	human leukocyte antigen DR isotype
HSP	heat-shock protein
ICI	immune checkpoint inhibitor
IDO-1	indoleamine 2,3-dioxygenase 1
IFN	interferon
IL	interleukin
IMC	immature myeloid cells
iRECIST	immunotherapy Response Evaluation Criteria in Solid Tumours
JAK	Janus kinase

LAG-3	Lymphocyte-activation gene 3
LAL	Limulus Amebocyte Lysate
LOX-1	lectin-type oxidized LDL receptor-1
LPS	lipopolysaccharide
LRP1	lipoprotein receptor-related protein-1
LSECtin	liver and lymph node sinusoidal endothelial cell C-type lectin
M	monocyte
mAb	monoclonal antibodies
MACS	magnetic-activated cell sorting
MAPK	mitogen-activated protein kinase
MB	myeloblasts
MCL 1	myeloid cell leukemia sequence 1
MDP	monocyte-dendritic progenitor cells
MDSC	myeloid-derived suppressor cells
MEK	mitogen-activated protein kinase kinase
MHC	major histocompatibility complex
miRNA	micro ribonucleic acid
M-MDSC	monocytic MDSC
MMP9	matrix metalloproteinase 9
MyD88	myeloid differentiation primary response 88
NF- κ B	nuclear factor kappa-light-chain-enhancer of activated B cells
NK	natural killer
NO	nitric oxide
OS	overall survival
P/S	penicillin/ streptomycin
PBMC	peripheral blood monocyctic cells
PBS	phosphate-buffered saline
PD-1	programmed cell death protein 1
PDE5	Phosphodiesterase 5
PD-L1	programmed cell death ligand 1
PFS	progression-free survival
PGE-2	prostaglandin E2
PMN-MDSC	polymorphonuclear MDSC
PVDF	polyvinylidene-difluoride
r	recombinant
RNA	ribonucleic acid
ROS	reactive oxygen species
RT	radiation therapy
RT-PCR	quantitative real-time PCR
S100	S100 calcium-binding protein
SDS	sodium dodecyl sulfate
SDS-PAGE	SDS polyacrylamide gel electrophoresis
Src	proto-oncogene tyrosine-protein kinase Src
STAT	signal transducer and activator of transcription
TAM	tumor-associated macrophages
TAN	tumor associated neutrophils
TBS	Tris-buffered saline
TCR	T cell receptor
TGF- β	transforming growth factor β
TEV	tumor-derived EV
TIGIT	T cell immunoreceptor with Ig and ITIM domains

TIM-3	T-cell immunoglobulin and mucin-domain containing-3
TLR	toll-like receptor
TME	tumor microenvironment
TNF	tumor necrosis pathway
TRAIL	TNF related apoptosis inducing ligand
Trap1	TNF receptor-associated protein 1
Treg	regulatory T cells
T-VEC	talimogene laher-parepvec
UV	ultraviolet
VEGF	vascular endothelial growth factor

2 SUMMARY

Tumor cells can modulate host immunity by secreting extracellular vesicles (EV) and soluble factors in the circulation. Uptake of these factors by myeloid cells or triggered signaling can lead to the generation of myeloid-derived suppressor cells (MDSC), which suppress anti-tumor activities of T and natural killer (NK) cells. Mouse and human melanoma-derived EV can induce this immunosuppressive activity by upregulating the expression of programmed cell death ligand 1 (PD-L1) on myeloid cells. This process was demonstrated to be dependent on the presence of heat-shock protein (HSP) 90 α in EV and on toll-like receptor (TLR) signaling. It is known that EV-associated or cellular HSP90 α could be a soluble serum compound. Here, we investigated whether HSP90 α as a soluble factor can convert human monocytes into MDSC.

Cluster of differentiation (CD) 14 monocytes were isolated from the peripheral blood of healthy donors, incubated with human recombinant HSP90 α (rHSP90 α) and analyzed by flow cytometry. Inhibition of T cell proliferation assay was used to assess immunosuppressive function of rHSP90 α -treated monocytes. Furthermore, levels of HSP90 α were measured by ELISA in plasma of melanoma patients and correlated with clinical outcome.

We found that upon 16 h incubation with rHSP90 α , monocytes strongly upregulated PD-L1 and indoleamine 2,3-dioxygenase 1 (IDO-1), while reactive oxygen species (ROS) and nitric oxide (NO) production, the expression of arginase-1 (Arg-1) as well as adenosine producing ectoenzymes CD39 and CD73 remained unchanged. The PD-L1 upregulation could be blocked by anti-TLR4 antibodies and nuclear factor kappa-light-chain-enhancer of activated B cells (NF- κ B) inhibitor. After longer incubation (for 24h), rHSP90 α -treated monocytes downregulated the expression of human leukocyte antigen DR isotype (HLA-DR). In addition, incubation with rHSP90 α led to an increased viability and prevention of apoptosis. Monocytes treated for 24 h with rHSP90 α acquired capacity to inhibit T cell proliferation in TLR4-, PD-L1-, and IDO-1-dependent manner. Higher levels of HSP90 α in plasma of melanoma patients

correlated with PD-L1 expression on blood-derived monocytic MDSC. Moreover, melanoma patients with higher levels of HSP90 α receiving immunotherapy displayed shorter progression-free survival.

This thesis highlights a possible mechanism of monocyte conversion into MDSC by a soluble HSP90 α , suggesting additional targets for overcoming immunosuppression in melanoma.

3 INTRODUCTION

3.1 Melanoma

Melanoma is characterized by fast progression, high invasiveness and potential to metastasize as well as by resistance to chemo- and radiotherapy¹. Current approach to the treatment of melanoma depends on the depth of invasion and the presence of locoregional and/or distant metastases². Wide excision with a sentinel lymph node biopsy is a standard of care for a localized disease. In case of a positive sentinel lymph node, complete lymph node dissection is recommended followed by adjuvant therapy. Neoadjuvant treatment for high-risk resectable melanoma has recently demonstrated improved progression-free survival and was approved for this group of patients³. Management of advanced/metastatic disease is mainly based on immune checkpoint inhibitor (ICI) treatment or targeted therapy for serine/threonine-protein kinase B-raf (BRAF) V600-mutated melanoma². Talimogene laherparepvec (T-VEC) represents an additional option for unresectable melanoma stage IIIB/C, IVM1a⁴. Despite the advances in survival of melanoma patients upon the treatment with the modern therapies, various resistance mechanisms still challenge the research community^{5,6}.

3.2 ICI in melanoma

ICI therapy is based on the fact that although melanoma is highly immunogenic due to the high mutational burden, clinically detectable tumors successfully escape host response by various mechanisms including but not limited to immune checkpoints⁷⁻⁹. Therefore, blocking immune checkpoints like PD-L1 and/or cytotoxic T-lymphocyte-associated protein (CTLA)-4 restores existing but hampered anti-tumor immune response⁶.

In order to evade immune surveillance despite ICI, melanoma cells can imply such mechanisms as disruption of antigen presentation or secretion of PD-L1-bearing EV^{10,11}. Several approaches to increase ICI efficacy by targeting melanoma cells have been implicated, including combination of ICI with targeted therapy, radiation therapy, T-VEC and metformin

(Figure 1)¹²⁻¹⁵. To evade host immune responses and undermine ICI therapeutic attempts, melanoma induces an immunosuppressive tumor microenvironment^{8,9}.

3.3 The tumor microenvironment (TME)

To generate an immunosuppressive milieu, melanoma cells secrete multiple factors that systemically induce the generation of immunosuppressive cells such as MDSC, regulatory T cells (T_{reg}), tumor-associated macrophages (TAM), cancer-associated fibroblasts (CAF), etc. and recruit them to the tumor site^{8,9}. Balance between effector and immunosuppressive cells within the TME was demonstrated to determine the effectiveness of immune-checkpoint inhibitors and thereby prognosis for melanoma patients^{6,16-18}. Each cell type in the TME represents a promising target for a monotherapy or a therapy in combination with ICI (Figure 1).

CAF promote tumor progression by shaping the tumor stroma and their accumulation was also associated with diminished efficacy of ICI¹⁹. An agent targeting fibroblast activation protein (FAP) is being studied in a clinical trial (NCT03875079) in combination with pembrolizumab.

Tumor-associated neutrophils (TAN) can promote tumor angiogenesis and metastasis and were associated with reduced progression-free survival (PFS) and overall survival (OS) in ICI-treated melanoma patients^{20,21}. Four strategies are being developed to target TAN: depletion, re-differentiation, inhibition of recruitment, and functional blockade²². Still a major challenge is the phenotypical distinction of tumor-promoting neutrophils from healthy neutrophils²².

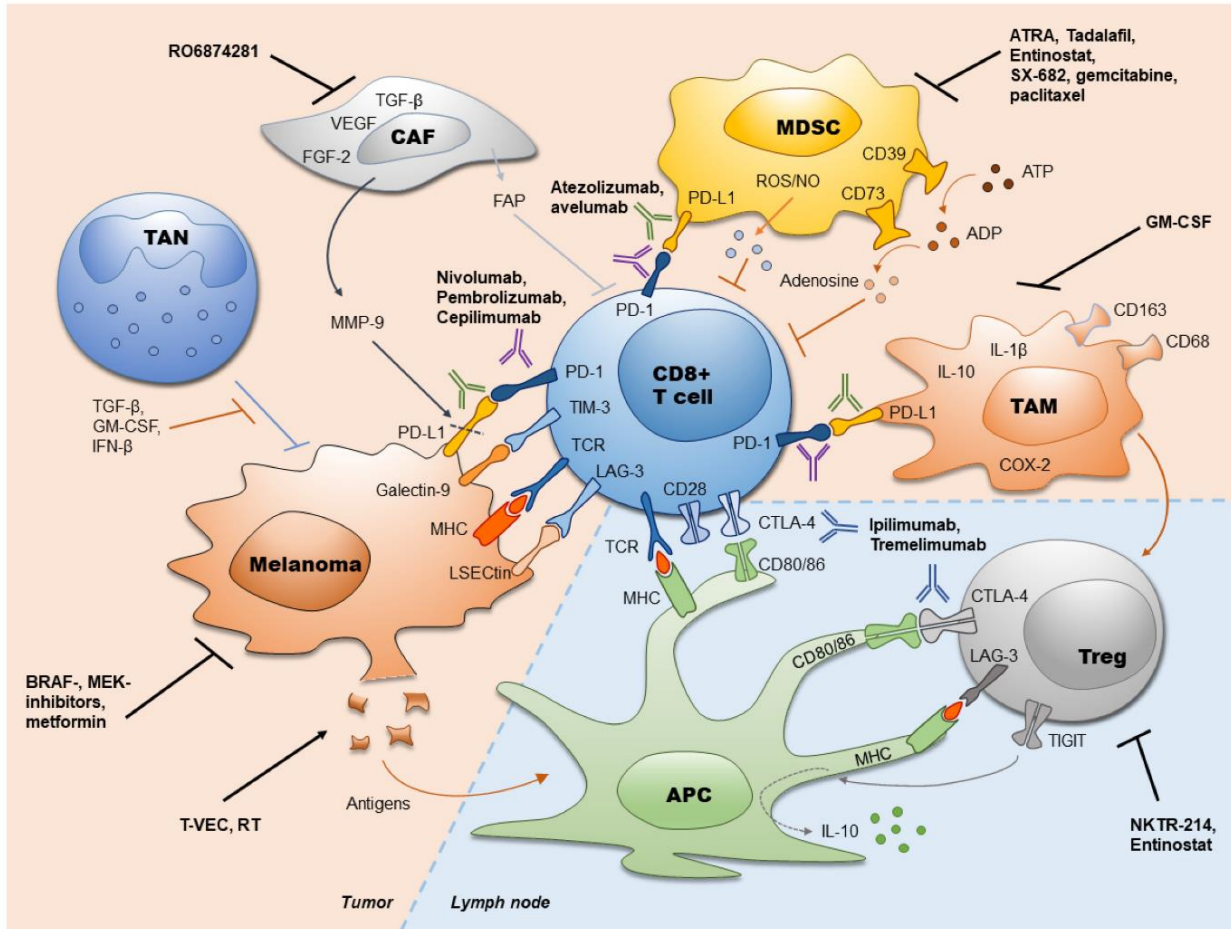


Figure 1. Immune checkpoint inhibitors in melanoma and their combination with other therapies. Currently used antibodies against PD-1 (atezolizumab, avelumab), PD-L1 (nivolumab, pembrolizumab, cepilimumab) and CTLA-4 (ipilimumab, tremelimumab) as well as strategies to increase the efficiency of ICI are presented. Figure taken from Petrova et al.⁶ ADP – adenosine diphosphate, APC – antigen presenting cells, ATP – adenosine triphosphate, BRAF – serine/threonine-protein kinase B-raf, CAF – cancer-associated fibroblasts, CD – cluster of differentiation, COX2 – cyclooxygenase-2, CTLA4 – cytotoxic T lymphocyte-associated protein-4, FAP – fibroblast activation protein, FGF – fibroblast growth factor, GM-CSF – granulocyte-macrophage colony stimulating factor, IFN- β – interferon β , IL – interleukin, LAG-3 – Lymphocyte-activation gene 3, LSECtin – liver and lymph node sinusoidal endothelial cell C-type lectin, MDSC – myeloid-derived suppressor cells, MHC – major histocompatibility complex, MEK – mitogen-activated protein kinase kinase, MMP9 –

matrix metalloproteinase 9, NO – nitric oxide, PD-1 – programmed cell death protein 1, PD-L1 – programmed cell death ligand 1, ROS – reactive oxygen species, RT – radiation therapy, TAM – tumor-associated macrophages, TAN – tumor-associated neutrophils, TCR – T cell receptor, TGF- β – transforming growth factor β , TIGIT – T cell immunoreceptor with Ig and ITIM domains, TIM-3 – T-cell immunoglobulin and mucin-domain containing-3, Treg – regulatory T cells, T-VEC – talimogene laherparepvec, VEGF – vascular endothelial growth factor.

Treg abundance was shown to positively correlate with a poor prognosis in melanoma. Bempegaldesleukin (NKTR-214/BEMPEG), a CD122-preferential interleukin (IL) 2 pathway agonist, was developed to specifically activate CD8 T cells without a stimulatory effect on Treg and is being investigated in melanoma in combination with nivolumab²³.

CD163⁺ TAM were reported to maintain immunosuppression in an anti-programmed cell death protein 1 (PD-1) resistant mouse melanoma model and their specific depletion led to activation of T cells and tumor regression²⁴.

Another important player in the TME is MDSC subset²⁵.

3.2.1 MDSC

MDSC are generated from myeloid progenitors upon unresolved inflammation in cancer and can be classified into two main subpopulations: monocytic MDSC (M-MDSC) and polymorphonuclear MDSC (PMN-MDSC)²⁵. In human, M-MDSC are defined as CD33^{high}CD14⁺HLA-DR^{low/-} and PMN-MDSC as CD33^{dim}HLA⁻DR^{neg}CD66b⁺²⁶. An additional more immature MDSC subset named early-MDSC was described as HLA-DR⁻CD33⁺CD15⁻CD14⁻ cells that do not exert suppressive activity²⁶. The distinction of PNM-MDSC from non-suppressive neutrophils remains challenging. Therefore, a relatively new

marker, lectin-type oxidized LDL receptor-1 (LOX-1), was proposed for the definition of PMN-MDSC in cancer patients²⁷. The Difference between M-MDSC and TAM is that M-MDSC are considered to be immature cells and TAM to be mature²⁵. TAM have specific surface cell marker signature (CD206⁺CD163⁺CD204⁺CD45⁺) and, in contrast to M-MDSC, do not express prostaglandin E2 (PGE-2) and S100 calcium-binding protein (S100) A8/A9²⁵.

Increased MDSC frequency was shown to be associated with poor survival in melanoma patients^{17,28-30}. Furthermore, higher peripheral blood levels of MDSC with elevated immunosuppressive capacity were found in melanoma patients who failed to respond to ICI treatment as compared to those who responded³¹.

Functionally active MDSC are thought to be absent in a healthy tissue. However, MDSC are accumulated during pregnancy in peripheral blood and decidua and serve as natural tolerogenic means for the embryo²⁵. MDSC expand in neonates and were shown to promote excessive inflammation in mouse models of newborns' microbial infection³².

Expansion of MDSC is promoted by hematopoietic growth factors and cytokines that have pro-inflammatory activity and can generate antitumor responses by activating dendritic cells (DC) in case of acute inflammation³³⁻³⁵. Tumors hijack these mechanisms and exploit them to generate pro-tumorigenic myeloid cells^{34,35}. To the mentioned factors belong granulocyte-macrophage colony-stimulating factor (GM-CSF), monocyte (M)-CSF, granulocyte (G-) CSF, IL-6, interferon (IFN)- γ , IL-1 β , IL-10, and vascular endothelial growth factor (VEGF) as well as TLR ligands that are constantly produced by tumors^{34,36}. Major source for MDSC generation are myeloid progenitors including monocyte-dendritic progenitor cells (MDP) or myeloblasts (MB)^{25,37}. However, generation of suppressive myeloid cells can also occur in cancer as a result of conversion of circulating monocytes³⁸⁻⁴⁰.

Generation of MDSC is thought to be a two-step process. First, cells get a pro-survival signal GM-CSF, G-CSF, M-CSF, IL-6 and VEGF signaling, through Janus kinase (JAK)/signal transducer and activator of transcription (STAT) and mitogen-activated protein kinase (MAPK) pathways that upregulate anti-apoptotic factors like Cyclin D1, Survivin, B cell lymphoma-extra-large (Bcl-xL), and c-Myc³⁴. Second, MDSC are activated by IFN- γ , IL-1 β and TLR ligands, mainly via JAK/STAT and myeloid differentiation primary response 88 (MyD88)/NF- κ B signaling that upregulate immunosuppressive factors³⁴. An additional important mechanism of MDSC generation is mediated by tumor-derived EV⁴¹ the role of which is described below.

Next, generated MDSC need to be recruited to the tumor site. This occurs predominantly by chemokines secreted by tumors. M-MDSC are primarily recruited by C-C motif ligand (CCL) 2, CCL3, CCL4 via C-C chemokine receptor type (CCR) 2 and PMN-MDSC are recruited by numerous ligands of CXC chemokine receptor (CXCR) 2⁴²⁻⁴⁴. A series of studies from our lab have demonstrated the role of CCR5 in the recruitment and further activation of MDSC in melanoma^{45,46}.

Immunosuppressive activity of MDSC is conducted via multiple mechanisms such as expression of a negative immune regulator PD-L1, Fas ligand (FasL), ID, production of suppressive ROS, NO, adenosine, depletion of L-arginine by Arg-1, and by induction of Treg and M2 populations^{47,48}. MDSC are able to inhibit adaptive immune cells like antigen-specific CD8 T cells and B cells as well as innate immune cells like NK cells⁴⁷.

Targeting of MDSC in cancer is complex and includes regulation of myelopoiesis, blockade of MDSC recruitment and inhibition of their immunosuppressive activity⁴⁹.

Depletion of MDSC by regulating myelopoiesis can be achieved for example by using all-trans retinoic acid (ATRA), which upregulates glutathione synthase, neutralizes high ROS production, and induces differentiation of MDSC into DC^{50,51}. MDSC depleting efficacy of ATRA was confirmed in clinical trials in renal carcinoma and small cell lung cancer

patients^{50,52}. Depletion of MDSC can be also achieved by ultra-low, non-cytotoxic doses of paclitaxel that was shown to downregulate MAPK pathway, production tumor necrosis pathway (TNF)- α and S100A9 and induce differentiation of MDSC into DC^{53,54}.

Recruitment of MDSC to the tumor site can be blocked by interfering with chemokine signaling^{44,46}. CCR5-Ig fusion protein that blocks all three CCR5 ligands was demonstrated to decrease the amount of circulating and tumor-infiltrating MDSC in melanoma mouse model and prolong survival of mice⁴⁶. CXCR2 inhibitor was demonstrated to decrease the tumor infiltration by PMN-MDSC, increase accumulation of NK cells, and prolong survival of melanoma-bearing mice⁴⁴.

Several agents have been demonstrated to block the immunosuppressive activity of MDSC⁴⁹. Phosphodiesterase 5 (PDE5) inhibitors tadalafil and sildenafil were found to diminish MDSC function as well as recruitment in mouse tumor models including melanoma⁵⁵⁻⁵⁷. Tadalafil demonstrated increase of antitumor immunity, reduction of MDSC and benefit for the prognosis for head and neck and melanoma patients⁵⁸⁻⁶⁰. A class I histone deacetylase inhibitor entinostat has shown activity against MDSC in preclinical cancer models and improved anti-PD-1 treatment^{61,62}. Another modality to hamper MDSC activity offers STAT3 inhibition. Napabucasin, a STAT3 inhibitor, was demonstrated to prolong the survival of melanoma-bearing mice and to abrogate immunosuppressive capacity of mouse and human *in vitro* generated MDSC⁶³.

3.2.2 Crosstalk between tumor and myeloid cells by means of extracellular vesicles

An outstanding role in the modulation of myeloid cells in tumors is played by EV secreted by tumor cells in TME and in circulation⁴¹. EV represent a heterogeneous group of secreted membrane vesicles, among which exosomes attracted a broad attention as mediators of intercellular communication⁶⁴. Exosomes are defined as EV of 50-150 nm size that have endosomal origin. Another group of EV is macrovesicles that derive from cellular membrane

and have size from 50 to 1000 nm⁶⁴. Interaction between tumor-derived EV (TEV) and different subsets of myeloid subsets is multifaceted, includes triggering of surface signaling or cargo delivery and have different outcomes depending on the source of TEV, the interacting EV-associated molecule and the recipient cells (Figure 2)⁴¹.

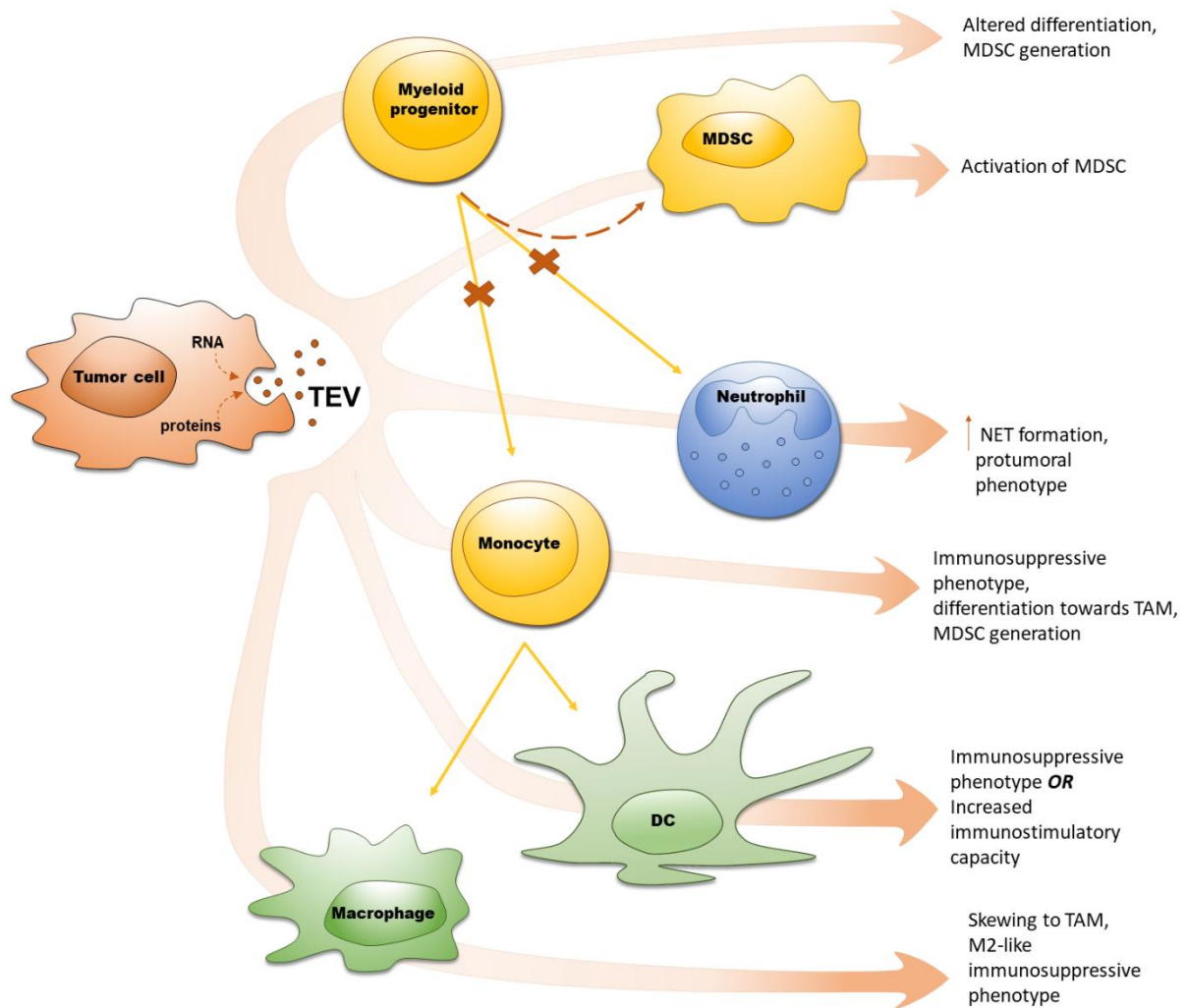


Figure 2. Tumor-derived extracellular vesicles (TEV) affect myeloid cell differentiation and function. Tumor cells secrete TEV containing tumor-derived factors (proteins, mRNA, miRNA etc.), which interact with myeloid progenitors (partially blocking their differentiation to mature myeloid cells that is shown with “x”), monocytes, neutrophils and MDSC, resulting in tumor-promoting immunosuppression (shown with arrows). Exposure of DC to TEV leads to the acquisition of immunosuppressive function or induction of immunostimulatory capacity (shown with arrows) Figure taken from Arkhypov et al.⁴¹ DC – dendritic cells, MDSC –

myeloid-derived suppressor cells, RNA – ribonucleic acid, TAM – tumor-associated macrophages.

It was shown that injection of hepatocellular carcinoma (HCC) bearing mice treated with sorafenib and anti-PD-1 antibodies with DC treated with EV generated from murine cell line of HCC led to the decrease of Treg count and increased survival of mice⁶⁵. EV isolated from murine cell lines of breast cancer and colon cancer containing micro ribonucleic acid (miRNA)-155, miRNA-142 or let-7i can enhance maturation of DC and increased stimulation of T cells^{66,67}. However, EV derived from murine cell lines of lung, breast, thymic, and skin tumors could hamper DC maturation, diminish their migration capacity to the draining lymph nodes and even to bring on immunosuppressive phenotype^{68,69}.

Macrophages can acquire immunosuppressive phenotype in a STAT-3 dependent manner upon the treatment with EV isolated from murine cell lines of skin, ovarian, liver cancer, and glioma⁷⁰⁻⁷⁴. Effects from these studies were linked to the EV-associated miRNAs: let-7a, miRNA-1246, miRNA-222, miRNA-146a, and miRNA-23a⁷⁰⁻⁷⁴.

While for DC and macrophages, EV uptake can lead to the phenotype switch, for MDSC, it can lead to the augmentation of the given suppressive phenotype⁴¹. Several miRNAs (miRNA-10a, miRNA-21, miRNA-29a, miRNA-92a, miRNA-107, miRNA-155) were linked to EV-mediated expansion and activation of MDSC due to an increased expression of Arg-1 and PD-L1⁷⁵⁻⁷⁹. In addition to miRNA, HSP70 and HSP72 found in association with TEV derived from different tumor cells could trigger TLR2-STAT3 signaling leading to the activation of MDSC, cytokine release and tumor progression⁸⁰⁻⁸³.

DC, macrophages and MDSC reside predominantly in tissues and are exposed to TEV *in vivo* within the TME or via lymphatics. In the circulation, TEV could affect monocytes or, myeloid progenitor cells in the bone marrow. Interaction of TEV with myeloid progenitor cells

was demonstrated to block their differentiation and led to the accumulation of MDSC^{69,84,85}. One study reported that TEV from poorly metastatic melanoma can induce “patrolling” monocytes able to recruit NK cells and induce TNF related apoptosis inducing ligand (TRAIL)-dependent killing of melanoma cells by macrophages leading to cancer surveillance at the pre-metastatic niche⁸⁶. Other studies demonstrated that the uptake of TEV derived from human cell lines of colorectal, cancer, pancreatic, gastric cancer and malignant brain tumor by monocytes induced an immunosuppressive phenotype⁸⁷⁻⁹¹. Furthermore, a set of miRNAs (miRNA-146a, miRNA-155, miRNA-125b, miRNA-100, let-7e, miRNA-125a, miRNA-146b, miRNA-99b) upregulated in ICI-resistant melanoma patients was found to be responsible for TEV-mediated conversion of monocytes into MDSC³⁸. In a previous work from our group, it was observed that the generation of MDSC from immature myeloid cells and from circulating human monocytes could be induced by melanoma-derived EV carrying HSP90 α ³⁹.

3.3 Heat-shock protein 90

HSP90 is a vital cellular chaperone that has two main isoforms: inducible HSP90 α and constitutive HSP90 β ⁹². HSP90 has an N-terminal domain with ATPase activity responsible for its chaperone function, a C-Terminal domain responsible for the formation of the functional HSP90 dimer and a middle domain⁹³. Specific isoforms of HSP90 are localized in mitochondria called TNF receptor-associated protein 1 (Trap1) and in endoplasmatic reticulum called 94-kDa glucose-related protein (Grp94)^{93,94}. In addition, HSP90 localized on the cell surface or secreted from the cytoplasm is termed extracellular HSP90 (eHSP90)⁹⁵. Beyond its function in protein folding, HSP90 takes part in various cellular processes like deoxyribonucleic acid (DNA) repair, neuronal signaling, immune response, cancer development and progression by chaperoning oncogenes⁹³. HSP90 is widely studied as a therapeutic target in oncology since it is overexpressed by all tumor cells⁹², including melanoma cells⁹⁶. Most currently available and investigated in clinical trials HSP90 inhibitors are directed against its N-terminal-chaperone

activity and are analogues of geldanamycin⁹³. Other approaches to inhibit HSP90 include C-terminal directed inhibitors (e.g. novobiocin) or chemically modified cell impermeable inhibitors that interact with eHSP90⁹⁴.

Since HSP90 is critical for functioning of normal cells, its inhibition is connected with prominent side effects. Finding the therapeutic window for HSP90 inhibitors, in which drugs are able to target cancer cells without large harm to healthy tissues was possible not only due to elevated levels of HSP90 in cancer but also due to HSP90 activation and ectopic localization on the cell membrane or in the extracellular space⁹⁷. Particular interest has eHSP90 due to its activity in wound healing, tissue fibrosis, and cancer (⁹⁸). Involvement of the extracellular HSP90 both in the wound healing and cancer progression corresponds to the hypothesis of tumors as “wounds that do not heal”^{99,100} since its promotility effects can lead both to tissue repair and to cancer invasion (Figure 3)⁹⁸.

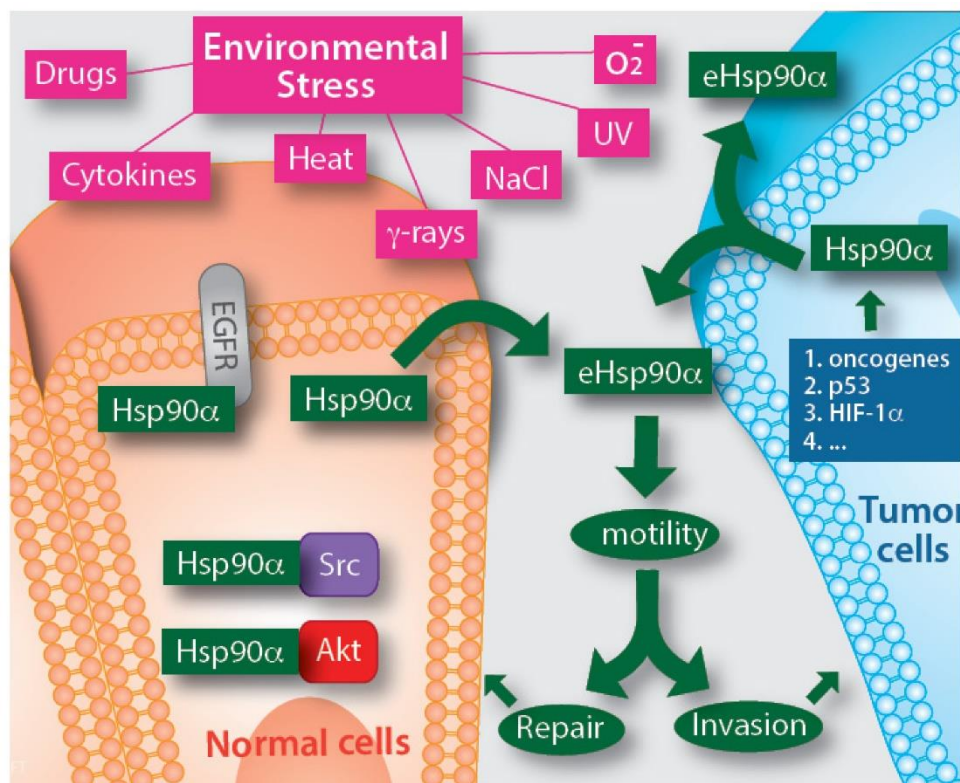


Figure 3. Secretion of HSP90 alpha isoform upon the stress conditions promotes tissue repair and cancer invasion. Different stress factors like reactive oxygen species, UV-light,

cytokines as well as several oncogenes and hypoxia inducible factor (HIF)1 α can lead to expression of HSP90 α isoform that has promotility effects in the extracellular space that are involved in tissue repair by normal cells and in invasion by cancer cells. Figure taken from Jay et al.⁹⁸. Akt – AKT serine/threonine kinase 1, EGFR – epidermal growth factor receptor, HSP90 – heat-shock protein 90, Src – proto-oncogene tyrosine-protein kinase Src, UV – ultraviolet.

With regard to the antitumor immunity, inhibition of HSP90 was shown to enhance T cell responses, prevent induction of MDSC, and improve ICI therapy^{101–104}. Increased T cell recognition of melanoma cells upon the treatment with twelve different HSP90 inhibitors was linked to the increased expression of major histocompatibility complex (MHC) class I antigens, most likely due to transcriptional activation¹⁰¹. Prevention of MDSC induction *in vitro* via HSP90 inhibitors was indicated by an increased HLA-DR expression and decreased immunosuppressive capacity in the co-culture with T cells¹⁰⁴. In addition, eHSP90 α was shown to upregulate the expression of IL-6 and IL-8 in prostate stroma fibroblasts mediated by NF- κ B and mitogen-activated protein kinase kinase (MEK) / extracellular-signal regulated kinase (ERK) signaling¹⁰⁵. Inhibition of HSP90 was demonstrated to synergize with cellular immunotherapy and with anti-CTLA4 and anti-PD1 therapy in injectable B16 and MC38 mouse melanoma models^{102,103}. Improved ICI efficacy upon HSP90 inhibition was linked to the upregulation of IFN response genes essential for T cell effector function¹⁰³.

In the extracellular space, HSP90 α was demonstrated to enhance cancer cell invasiveness and migration^{106–108}, induce activation of STAT3 and NF- κ B-dependent IL-6 and IL-8 production by prostate stromal fibroblasts¹⁰⁵ and promote metastasis formation^{109–111}. Plasma HSP90 α was suggested to be used as a pan-cancer biomarker¹¹² and as a prognostic indicator for immunotherapy^{113,114}.

3.4 Aim of the thesis

As described above, immunosuppression in melanoma represents a substantial factor in the disease progression and development of the resistance towards currently available therapeutics. One of the major players in immune evasion in melanoma are MDSC. A previous study from our group had shown that MDSC could be induced by HSP90 α -bearing TEV³⁹. In the present study, we aimed to investigate the possible mechanism of myeloid cell conversion into MDSC by soluble HSP90 α . For this purpose, we incubated human monocytes with recombinant HSP90 α . Phenotypical switch to immunosuppressive state was assessed by the expression of PD-L1, HLA-DR, and IDO-1 by means of flow cytometry and Western Blot. The ability of the stimulated cells to survive longer was studied in the apoptotic assay including Annexin V and 7-aminoactinomycin D (7-AAD) stainings. To reveal the mechanism of HSP90 α -mediated effects, we applied TLR4 blocking antibodies and the NF- κ B inhibitor Bay while treating monocytes with HSP90 α . Moreover, we performed microarray analysis of HSP90 α -treated monocytes for the comprehensive characterization of the stimulated cells. The immunosuppressive capacity of the HSP90 α -treated monocytes was proven by the inhibition of the T cell proliferation assay in the presence or absence of anti-PD-L1 blocking antibodies or the IDO-1 inhibitor 1-methyl-D-tryptophan (1-D-MT). Finally, we measured the level of HSP90 α in the plasma of advanced melanoma patients, its possible association with the OS and PFS as well as with the resistance to ICI therapy.

4 MATERIAL AND METHODS

4.1 Material

4.1.1 Protein expression and purification

Table 1: Reagents and equipment used for the protein expression and purification

Product	Company
Isopropyl β -d-1-thiogalactopyranoside	Carl Roth
0.45 μ m syringe filter	ROTILABO
Spin columns	Biozym
Ni-NTA superflow resin	Qiagen
Imidazole	Carl Roth
Slide-A-Lyzer dialysis cassette	Thermo Fisher
Immobilized TPCK-Trypsin	Thermo Scientific

4.1.2 Cell line

Table 2: Cell line used for the production of EV

Cell line	Source	Cell type	Mutation	Medium
HT-144	ATCC	Melanoma cell line	BRAF V600E	RPMI

4.1.3 Cell culture products

Table 3: Reagents used for cell culture

Product	Company
B-Mercaptoethanol (50 mM)	Gibco
Dimethylsulfoxid (DMSO)	Carl Roth
Dulbecco's phosphate-buffered saline (DPBS)	PAN Biotech

Fetal Bovine Serum	PAN Biotech, Gibco
HEPES Buffer	Gibco
MACS BSA Stock Solution (10 %)	Miltenyi Biotec
Human albumin	CSL Behring
MEM NEAA (100x)	Gibco
Penicillin/ Streptomycin (P/S)	Gibco
RPMI Medium 1640 (1x) + GlutaMAX™	Gibco
Sodium pyruvate (100 mM)	Gibco
UltraPure™ EDTA (0.5M, pH 8.0)	Gibco
Biocoll	Biochrom

4.1.4 Cell culture media

Table 4: Content of media used for cell culture

Name	Composition
Full RPMI Medium	500 ml RPMI Medium 1640 (1x) + GlutaMAX™
	10 % FBS
	1 % P/S
Serum free RPMI Medium	500 ml RPMI Medium 1640 (1x) + GlutaMAX™
	1 % P/S
Full Monocyte Medium	500 ml RPMI Medium 1640 (1x) + GlutaMAX™
	10 % FBS
	1 % P/S
	10 mM HEPES
	1 mM Sodium Pyruvate
	50 µM β-Mercaptoethanol

	1 mM MEM Non-essential amino acids
Low Arginine Medium	88 mL RPMI 1640 Medium for SILAC
	10 % FBS
	1 % P/S
	0.04 mg/mL L-Lysine hydrochloride
	0.15 mM L-Arginine

4.1.5 Kits

Table 5: Kits

Product	Company
Pierce LAL Chromogenic Endotoxin quantification Kit	Thermo Fisher
CD14 MicroBeads, human	Miltenyi Biotec
CD3 MicroBeads, human	Miltenyi Biotec
Human CD9 Capture Beads	Immunostep
Human CD63 Capture Beads	Immunostep
Permeabilisation Concentrate and Diluent	Invitrogen
SensiFAST™ SYBR® Lo-ROX Kit	Bioline
Human HSP90 α ELISA kit	Invitrogen, Bio-Techne
ROS detection kit	Cell Technology
Pierce™ BCA Protein Assay Kit	Thermo Fisher
RNeasy Mini kit	Qiagen
on-column RNase-free DNase set	Qiagen

4.1.6 Antibodies

Table 6: Primary antibodies

Name	Clone	Company
GAPDH	FF26A	Invitrogen
Mouse IgG2a kappa Isotype Control	eBM2a	Invitrogen
CD282 (TLR2) Antibody, Functional Grade	6C2	eBioscience
CD284 (TLR4) Antibody, Functional Grade	HTA125	eBioscience
IDO-1	D5J4E	Cell Signaling
HSP90 α	Polyclonal	Abcam

Table 7: Peroxidase-conjugated antibodies

Name	Clone	Company
Horseradish peroxidase (HRP)-conjugated goat anti-mouse	Polyclonal	Jackson Immuno Research
Peroxidase AffiniPure Goat Anti-Rabbit IgG (H+L)	Polyclonal	Jackson Immuno Research

Table 8: Fluorescent-conjugated antibodies

Name	Fluorophore	Clone	Company
CD14	FITC	M Φ P9	BD Biosciences
PD-L1	BV421	MIH1	BD Horizon
IgG1	BV421	X40	BD Horizon
HLA-DR	V500	G46-6	Biologend
HLA-DR	APC-H7	G46-6	BD Pharmingen
CD33	PE	WM53	BD Biosciences

CD39	APC	TU66	BD Pharmingen
CD73	BV605	AD2	Biolegend
ARG-1	PE	AlexF5	Invitrogen

4.1.7 Primers for mRNA

Table 9: Primers used for real-time PCR

Primer	Species	Orientation	Sequence
Bcl-2	Human	forward	5'-TTGTGGCCTTCTTTGAGTTCGGTG-3'
		reverse	5'-GGTGCCGGTTCAGGTACTCAGTCA-3'
Mcl-1	Human	forward	5'-AGAAAGCTGCATCGAACCAT-3'
		reverse	5'-CCAGCTCCTACTCCAGCAAC-3'
Bax	Human	forward	5'-CCTGTGCACCAAGGTGCCGGAAC-3'
		reverse	5'-CCACCCTGGTCTTGGATCCAGCCC-3'
Caspase3	Human	forward	5'-TCCTGAGATGGGTTTATGT-3'
		reverse	5'-ATGTTTCCCTGAGGTTTGC-3'

4.1.8 Chemicals and biological reagents

Table 10: Chemicals and biological reagents

Product	Company
10 % Tween® 20 Solution	BioRad
10 x Permeabilization Buffer	eBioscience
7-AAD Staining Solution	BD Biosciences, Miltenyi Biotec
ACK lysis buffer	Gibco
Acrylamide solution	Carl Roth

Amiloride,5'- (N, N-Dimethyl)-hydrochloride	Enzo
Ammonium persulfate	Sigma-Aldrich
Annexin V APC	Biolegend
Annexin V Binding Buffer (10X)	BD Biosciences
Albumin IgG free	Carl Roth
ATX Ponceau S red staining solution	Sigma-Aldrich
Carboxyfluorescein succinimidyl ester (CFSE)	Biolegend
Cell proliferation dye eFluor 450	BD Biosciences
Clear PAGE LDS sample buffer (4x)	Invitrogen
Glycine	Carl Roth
Highly sensitive ROS Detection Kit	Cell Technology
Isopropanol	Carl Roth
Fixable viability dye 700	BD Biosciences
Methanol	Carl Roth
NF- κ B Inhibitor Bay 11-7082	Sigma Aldrich
NO detection reagent (diaminofluoresceine-FM diacetate)	Cayman Chemical
PageRuler Protein ladder prestained	Thermo Fisher Scientific
Pierce® ECL Western Blotting Substrate	Thermo Fisher Scientific
Pierce® RIPA Buffer 100 ml	Sigma Aldrich
RBC Lysis Buffer (10x)	Biolegend
Sodium dodecyl sulfate (SDS)	Carl Roth
Temed	BioRad
TRIS	Carl Roth

Trizol ® Reagent	Life Technologies
Trypan Blue Solution	Sigma Aldrich

4.1.9 Solutions

Table 11: Content of solutions:

Name	Composition
Freezing medium 1	60 % FBS
	40 % X-VIVO 20
Freezing medium 2	75 % FBS
	25 % DMSO
1 x Tris-buffered saline (TBS)	5 mL 1 M Tris/HCl, pH 8
	15 mL 1 M NaCl
	470 mL ddH ₂ O
Stacking polyacrylamide gel	6 mL ddH ₂ O
	1.35 mL 30 % Acrylamide solution
	2.5 mL 0.5 M Tris/HCl, pH 6.8
	100 µL 10 % SDS
	100 µL 10 % APS
	10 µL TEMED
10 % Separating polyacrylamide gel	21.3 mL ddH ₂ O
	13.3 mL 30 % Acrylamide solution
	5.3 mL 3 M Tris/HCL, pH 8.8
	400 µL 10 % SDS
	133 µL 10 % APS
	TEMED

10 x Running buffer	30 g Tris base
	144 g Glycine
	10 g SDS
	10 L ddH ₂ O
10 x Blotting buffer	121.2 g Tris base
	576 g Glycine
	4 L ddH ₂ O
Blocking buffer for western blot	DPBS
	3 % BSA
	0.05 % Tween-20 in TBS
FACS buffer	DPBS
	2 % FBS
	0.2 % NaN ₃
MACS buffer	DPBS
	1% BSA
	0.5 mM EDTA

4.1.10 Routine laboratory material

Table 12. Description of the routine laboratory material

Product	Company
24-well flat bottom with lid	Greiner bio-one
96-well flat bottom with lid	TPP®
96-well U-bottom with lid	Sigma Aldrich
serological pipettes: 5, 10 and 25 mL, sterile	Greiner bio-one
15 mL conical tubes	Falcon

50 mL conical tubes	Falcon
Amicon® Ultra Centrifugal tube	Merck Millipore
Cell culture flasks T75	Sigma Aldrich
TC dish, 150 Standard	Sarstedt
Cryovial, 2 mL sterile	Sigma Aldrich
Filter tips: 20, 200, 1000 µL	Steinbrenner
Freezing Container, "Mr. Frosty"	Nalgene
Safe lock tubes: 0.5, 1.5 and 2 mL	Eppendorf
Syringe 1 mL	BD
Neubauer chamber	Brand
Stericup&Steritop 0.22 µM Millipore Express PLUS membrane	Merck Millipore
LeucoSep tubes	Greiner Bio-one
iBlot Transfer Stack	Thermo Fisher Scientific
ThickBlot Filter Paper	BioRad
PVDF membrane	Thermo Fisher Scientific
Insert, 24 well, PET 0.4 µm, TP	Sarstedt

4.1.11 Laboratory equipment

Table 13. Description of the laboratory equipment

Device	Name	Provider
Balance	BP 3100P	Sartorius
Cell culture incubator	Hera cell	Heraeus
Centrifuges	Biofugeprimor	Heraeus
	MEGAFUGE 40R	Heraeus

	Labofuge 400R	Heraeus
Confocal microscope	TCS SP2	Leica
Flow cytometer	FACS Lyric	BD Biosciences
Heating block	Digital Block Heater HX-2	Peqlab
Imaging system	Fusion SL	VilberLourmat
Laminar flow hood	Hera safe	Thermo Electron Cooperation
Magnetic stirrer	RCT basic	IKA Werke
Microplate Reader	Tecan infinite M200	Tecan
Microscope	DMIL	Leica
MACS Magnet and stand		Miltenyi Biotec
N2 tank	BIOSAFE® SC-smart	Cryotherm
Nanoparticle tracking system	Zeta View	Particle Metrix
Pipettes	Transferpette ® S	Brand
Power supply	PowerPac™ HC High Current	BioRad
Real-Time PCR machine	MX3005 qPCR System	Stratagene
Shaker	Logic shaker	NeoLab
Thermal Cycler	DNA Engine Peltier Thermal Cycler	BioRad
Transfer device	iBlot™ Gel Transfer Device	Thermo Scientific
Ultracentrifugation rotor	SW 32 Ti	Beckman Coulter
Ultracentrifuge	Optima XPN	Beckman Coulter
Vortexer	REAX top	Heidolph
	Vortex Genie 2	Scientific Industries

Water bath	DC3	HAAKE, GFL
------------	-----	------------

4.1.12 Software for data analysis

Table 14. List of software used for the data analysis

Product	Version	Company
Flow Jo	10.7.1	Tree Star Inc., Ashland, USA
GraphPad PRISM	8	GraphPad Software Inc., San Diego, USA
Mendeley Reference Manager	2.62.0	Mendeley
I control 1.10	1.10	TECAN

4.2 Methods

4.2.1 Cell culture

4.2.1.1 Cell counting

To determine the cell number, 10 μ L of the respective cell suspension were diluted in 90 μ L trypan blue (1:10). When necessary, 1:10 diluted suspension was diluted once more 1:10 in trypan blue (1:100). 10 μ L of the diluted suspension were transferred into a Neubauer chamber and live cells (trypan blue negative staining) were counted. Total cell number per mL was calculated using the following formula:

$$\text{live cell number per mL} = \frac{\text{number of trypan blue negative cells}}{\text{number of squares used for counting}} * 10^4 * \text{dillution factor}$$

4.2.1.2 Cell line expansion

Human melanoma cell line HT-144 was cultured in T75 flasks in a humidified incubator at 37°C and 5 % CO₂ in 15 mL full RPMI medium (Table 4) per flask. Cells were passaged at around 90% confluence. Cells were detached by incubating them with 3 mL of 1 x trypsin

containing 5 mM EDTA for 3 minutes at 37°C. To stop the trypsinization, 10 mL of full RPMI medium were added. Then cells were transferred into 50 mL tube, centrifuged at 300 g for 5 min. After discarding supernatant cells were split 1:10 into a new flask in required volume of medium (e.g. 30 mL for two T75 flasks).

4.2.1.5 Human blood processing: isolation and culture of PBMC, monocytes, T cells, M-MDSC; plasma collection

Peripheral blood monocyctic cells (PBMC) were isolated by density gradient using Biocoll separation medium (Biochrom) from healthy donors` buffy coats (German Red Cross Blood Service Baden-Württemberg-Hessen) or full blood from healthy donors or melanoma patients. 25 mL of the Buffy coat diluted 1;1 with sterile PBS or blood were overlaid on the 15 mL Biocoll and centrifuged at 400 g for 30 minutes without brake. Upper fraction of the formed gradient constituted plasma, the next part in form of a “ring” corresponded to PBMC, following part was the Biocoll, and the lower part contained erythrocytes and granulocytes. Plasma was collected leaving 5-10 mm over the PBMC “ring” and stored at -20°C or -80°C for further use. PBMC “ring” was collected accurately without taking up Biocoll and proceeded for the further isolation of monocytes, T cells or MDSCs.

CD14 monocytes and CD3 T cells were isolated from PBMC by magnetic beads as described in the section “Magnetic-activated cell sorting”. Monocytes were cultured in the full monocyte medium (Table 4). And treated with rHSP90 α at concentration of 2 $\mu\text{g}/\text{mL}/10^6$ cells or with respective volume of phosphate-buffered saline (PBS) (control) for 16, 24, and 48 hours.

For isolation of patient-derived monocytes and M-MDSC, PBMC were labelled with anti-human- CD33 and HLA-DR monoclonal antibodies (mAb). Monocytes (CD33⁺HLA-DR⁺) and M-MDSC (CD33⁺HLA-DR⁻) were purified by fluorescence-activated cell sorting (FACS Aria, BD Biosciences) by Flow Core Team (University Medical Center Mannheim, Germany).

4.2.1.6 Freezing and thawing

HT-144 melanoma cells were harvested at 80-90% confluence, centrifuged, resuspended in 2.5 mL full RPMI medium and mixed with 2.5 mL of freezing solution (20% DMSO, 80% FBS). Cell suspension was distributed into freezing tubes (1 mL/tube) and frozen in Mr. Frosty™ filled with isopropanol for 24 hours. Next, freezing tubes were transferred to the liquid nitrogen tank for a long-term storage.

For thawing, freezing tubes were put in 37°C water bath. Then cells were rapidly washed with 10-15 mL full RPMI medium and transferred into T75 flask for further culture. Cells were used for experiments between 2 and 10 passages after thawing.

4.2.2 Nucleic acid analysis

4.2.2.1 RNA isolation and cDNA synthesis

Total RNA was isolated from 2.5×10^6 monocytes using the RNeasy Mini kit (Qiagen) according to manufacturer's instructions. Digestion of DNA was performed using the on-column RNase-free DNase set (Quiagen). Isolated RNA was eluted in 25µL of RNase-free water. RNA concentration was measured by photometry at microplate reader Tecan Infinite M200 using the Nanoquant plate. For the storage RNA was frozen at -80°C.

4.2.2.2 RT-PCR

RNA from each sample was adjusted for the amount (up to 1 µg) and used for cDNA synthesis using the SensiFAST™ cDNA synthesis kit (Bioline) according to manufacturer's instructions. Following controls were used for exclusion of DNA contamination or contamination of the reagents: “noRT control” with RNA and without reverse transcriptase and “H₂O control” without RNA and with reverse transcriptase. All further steps were performed on ice.

Quantitative real-time PCR (RT-PCR) was performed using the SYBR Green Master Mix (Applied Biosystems, Life technologies) on a Stratagene Mx3005P real-time PCR system.

cDNA and controls were diluted with RNase-free water 1:55. 2 μ M of forward and reverse primers were mixed in equal amount. For the master mix 10 μ L diluted cDNA, 7 μ L primer mix and 17 μ L SensiFAST™ SYBR® Lo-ROX Kit (Bioline) were mixed together. 10 μ L of the master mix were transferred to three wells of a 96-well qPCR plate. Sealed plate was transferred into the Stratagene MX3005P qPCR machine for the amplification using the program displayed in the Table 15. Quantification of a relative gene expression was done by calculating $\Delta\Delta$ Ct. 18s was used as a housekeeping gene in all experiments for normalization.

Table 15: mRNA amplification program

Step	Temperature [°C]	Time [s]	Cycles
1	50	120	1
2	95	10	42
3	59-63	60	42
4	95	60	1
5	65	30	1
6	95	30	1

4.2.2.3 Microarray analysis

RNA collection for the microarray analysis was done by Feyza Gül Özbay Kurt and the microarray analysis was performed by Thomas Hielscher (Division of Biostatistics, German Cancer Research Center (DKFZ), Heidelberg, Germany). Total RNA was isolated from purified CD14 human monocytes treated with rHSP90 α or non-treated (control) by RNeasy Mini Kit (Qiagen) according to the manufacturer's instructions. RNA concentration was determined by the microplate reader Tecan Infinite M200 using a Nanoquant plate. For gene expression analysis, Affymetrix Clariom S human assay (Thermo Fisher Scientific) was applied according to the manufacturer's instructions. Affymetrix CEL files were RMA normalized and expression

values log₂-transformed. Differentially expressed genes in experimental groups were identified using the empirical Bayes approach¹¹⁵ based on moderated t-statistics as implemented in the Bioconductor package limma¹¹⁶ accounting for batch effects. Gene set enrichment analysis was performed using the camera test¹¹⁷. KEGG¹¹⁸, Reactome¹¹⁹ and Gene Ontology³⁶ databases were used in pathway analysis. An enrichment map was used to visualize results from pathway tests. The analysis was performed with statistical software R Statistical Software (V.4.0; R Core Team 2020) using the add-on package Enhanced- Volcano, and p values were adjusted for multiple testing using the Benjamini-Hochberg correction.

4.2.3 Protein analysis

4.2.3.1 Protein isolation

For the protein isolation, single cell suspension was washed with PBS once and centrifuged at 300 g for 5 minutes. The cell pellet was resuspended in 300 µL RIPA buffer containing protease inhibitor cocktail and incubated for 30 minutes at 4°C on a shaking platform. Next, lysate was centrifuged at 13,000 g for 15 minutes at 4°C. Protein-containing supernatant was transferred into a fresh Eppendorf tube and frozen at -20°C till further use.

4.2.3.2 Bicinchoninic acid (BCA) assay

Pierce® BCA Protein Assay Kit was used for measuring protein concentration. Given albumin standard was diluted to final concentrations of 2000 µg/mL, 1500 µg/ml, 1000 µg/ml, 750 µg/ml, 250 µg/ml, 125 µg/ml and 25 µg/ml with PBS. 10 µL of a sample, a standard, and PBS as a blank were pipetted in duplicates into a flat bottom 96-well plate. 200 µL of the BCA reagent A diluted 1:50 with the BCA reagent B were added to each well, the plate was sealed and incubated at 37°C for 30 minutes shaking. Afterward, the absorbance was measured using the Tecan Infinite M200 microplate reader at 562 nm.

4.2.3.3 Gel electrophoresis

Analyzed samples were equalized according to the protein concentration, mixed 1:4 with 4x Lämmli buffer and heated at 95°C for 5 minutes. Samples were loaded onto the 10% SDS polyacrylamide gel electrophoresis (SDS-PAGE) in a gel electrophoresis tank containing 1x running buffer. Electrophoresis was performed at 90V for 15 minutes followed by 120V for 45 minutes.

4.2.3.4 Western Blot and immunostaining

After the separation with SDS-PAGE, samples were blotted onto a polyvinylidene-difluoride (PVDF) membrane and a semi-dry blotting technique was used. PVDF membrane was activated in methanol for 1 minute, rinsed with water and blotting buffer and placed on top of the three waterman papers pre-soaked in blotting buffer. The SDS-gel was soaked in blotting buffer and transferred onto the PVDF membrane followed by another three sheets of waterman papers pre-soaked in blotting buffer. 0.6 mA/gel were applied for 90 minutes for transferring proteins. When needed, transfer of the proteins was checked by Ponceau S staining.

For the immunostaining, PVDF membrane was firstly blocked with 3% BSA in TBT-Tween at room temperature on the shaking platform. Next, the membrane was incubated with the primary antibody diluted in the 3% BSA in TBT-Tween either overnight at 4°C or for 1 h at room temperature followed by three 10 minutes washing steps with TBS-T. Washed membrane was then incubated with the HRP-conjugated secondary antibody diluted in 3 % BSA in TBS-T at same conditions as the primary antibody followed by the same washing steps. At the end, the membrane was treated for 1 min with Pierce® ECL Western Blotting Substrate at room temperature, and chemiluminescence was detected using the Fusion SL detection device.

4.2.3.5 Coomassie staining

Following an SDS-PAGE the gel was stained with Coomassie staining solution (0,1% (w/v) Coomassie brilliant blue R250 (Sigma-Aldrich), 10% acetic acid, 40% ethanol) for 10

min and afterwards destained with destaining solution (10% acetic acid, 30% ethanol) until the bands nicely stood out against the background.

4.2.3.6 Enzyme-linked immunosorbent assay (ELISA)

Plasma of melanoma patients and healthy donors for ELISA was collected after the density gradient centrifugation of the whole blood as described above. Measurement of HSP90 α was performed an ELISA kit from Invitrogen, Cat. # BMS2090 or Bio-Techne Cat. # NBP2-29914 according to the manufacturer's protocols. Briefly, plasma samples and HSP90 α protein standards were loaded into 96-well plates pre-coated with anti HSP90 α capturing and incubated with biotinylated anti-HSP90 α antibodies. Streptavidin-conjugated horseradish peroxidase was then added followed by substrate solution. Finally, enzyme reactions were stopped and OD450 values were measured by Infinite M200 microplate reader (TECAN).

4.2.4 Protein expression and purification

The plasmids encoding human HSP90 α and subfragments F-5 and F-6 covering the central M domain of HSP90 α were provided by Prof. Wei Li, Los Angeles, USA¹⁰⁷. The following steps of the protein expression and purification were performed by Daniel Novak PhD. The plasmid was transfected into Single Step (KRX) Competent E. coli cells (Promega) and protein expression was induced by adding IPTG (final concentration 1 mM) and rhamnose (final concentration 0.1%). After overnight culture, cells were harvested by centrifuging at 4000 g for 5 min and resuspending the pellet in lysis buffer (1.5% Triton X-114, NaH₂PO₄ 50 mM, NaCl 300mM, imidazole 10 mM, pH 8,0). Afterwards, the cells were lysed mechanically with a French Press. Lysate was centrifuged at 10,000 g and 2-8°C for 30 min. The supernatant was collected and filtered through a 0.45 μ m syringe filter (ROTILABO). 1 ml of 50% Ni-NTA agarose slurry (Qiagen) was loaded onto a PureCube 1-step batch Midi Plus Column (Biozym) and washed twice with lysis buffer by centrifuging at 400 g and 4°C for 5 min and discarding the flow-through. Then, the supernatant containing the rHSP90 was applied to the column with the Ni-NTA agarose and incubated over night at 4°C on a shaker. The next day, the supernatant

was centrifuged at 400 g and 4°C for 5 min and the flow-through was discarded. The beads were washed twice with washing buffer supplemented with Triton-X 114 (1.25% Triton X-114, NaH₂PO₄ 50 mM, NaCl 300mM, imidazole 20 mM, pH 8,0) to minimize the LPS contamination followed by two wash steps with washing buffer without Triton-X 114^{120,121}. Next, His-tagged proteins were eluted from the Ni-NTA beads five times with elution buffer (NaH₂PO₄ 50 mM, NaCl 300mM, imidazole 500 mM, pH 8,0).

The purity of recombinant protein was confirmed by the Coomassie staining and Western Blot. Peak fractions were pooled, concentrated and rebuffered into the storage buffer (NaH₂PO₄ 50 mM, NaCl 50mM, 2-mercaptoethanol 50 mM, 20% glycerol) by using Amicon® Ultra-15 Centrifugal Filter Devices (Millipore) according to the manufacturer's instructions. Protein concentration was determined with the Pierce™ BCA Protein Assay Kit (Thermo Fisher Scientific) according to the manufacturer's instructions. The rebuffered and concentrated protein solution was passed through a 0.45 µm syringe filter (ROTILABO), aliquoted, snap-frozen in liquid nitrogen and stored at -80°C. Expression of rHSP90α was confirmed by Western Blot and mass spectrometry. Measurement of the residual LPS contamination was performed by Limulus Amebocyte Lysate (LAL) (Pierce LAL Chromogenic Endotoxin quantification Kit, Thermo Scientific) according to manufacturer's instructions. As an additional quality check, trypsin on-beads digestion (Immobilized TPCK-Trypsin, Thermo Scientific) of the rHSP90α was performed according to manufacturer's instructions.

4.2.5 Magnetic-activated cell sorting (MACS)

CD14 monocytes and CD3 T cells were purified from PBMC by magnetic beads according to the manufacturers' instructions (Miltenyi). PBMC were washed with PBS and resuspended in 80 mL MASC buffer (Table 11) per 10⁷ cells. 20 µL of MACS CD14 or CD3 MicroBeads were added per 10⁷ cells, mixed, and incubated for 15 min at 4°C. Cell were than washed by adding 10–20x the labeling volume of buffer and centrifuging at 300g for 10 min. Supernatant was removed completely and the pellet was resuspended in 1 mL MACS buffer.

Magnetic separation was performed with positive selection LS columns moisten with 3 mL MACS buffer and installed into magnetic separator. After passing the cell suspension through the column, the column was rinsed three times with 3 mL MACS buffer. Column was then removed from separator and placed on a suitable collection tube. 5 mL of MACS buffer was pipetted onto the column and positive cells were flushed out using the plunger supplied with the column. Cells were washed again with MACS buffer and resuspended in medium for further analysis. Cell purity was >90% as checked by the flow cytometry.

4.2.6 Fluorescence-activated cell sorting (FACS) analysis

4.2.6.1 Surface staining

Cells (1×10^5 cells/well) were washed with PBS and treated with the cocktail of FcR Blocking reagent (Miltenyi Biotec) and Fixable viability dye 700 dissolved in PBS for 15 minutes at 4°C. Then, cells were washed with PBS again and stained with fluorescent-conjugated antibodies dissolved in FACS buffer (Table 11) for 20 min at 4°C. Afterwards, cells were washed in FACS buffer and resuspended for acquisition in 100 μ L FACS buffer. Antibodies and reagents used for flow cytometry staining are listed in the Tables 8 and 10. Acquisition was performed using FACS Lyric (BD Biosciences). Acquired data were analyzed by FlowJo software (Tree Star).

4.2.6.2 Reactive oxygen species (ROS) and nitric oxide (NO) detection

It was used the protocol for the surface staining with the modifications, i.e., the staining was performed in PBS and acquisition was done immediately after the staining was finished. ROS and NO detection reagents are listed in the Table 9.

4.2.6.3 Apoptosis assay

Monocytes were stained for surface markers as described above. Then, cells were washed and resuspended in 100 μ L Ca^{2+} -containing binding buffer at a concentration of 1×10^5 cells/well. Annexin V and 7-AAD were added according to the manufacturer's instructions.

Cells were further incubated for 15 min at room temperature. After incubation, cells were resuspended in 400µL/tube of Ca²⁺-containing binding buffer and analyzed by flow cytometry.

4.2.6.3 Intracellular staining

Monocytes were stained for surface markers as described above. Then, cells were washed cells with 150 µl FACS Buffer at 300 g, 5 min, 4 °C. Supernatant was discarded and cell were resuspended in 100 µL fixation/permeabilization working solution (eBioscience) and incubated for 30 min at 4 °C in the dark. Cells were washed with 150 µL permeabilization buffer (eBioscience) at 400 g, 5 min, 4 °C and resuspended in 100 µL of anti-Arg-1 antibody dissolved in permeabilization buffer and incubated 30 min at room temperature in the dark. Cells were washed with 150 µL permeabilization buffer at 300 g, 5 min, 4 °C and resuspended in 100 µL permeabilization buffer for the acquisition.

4.2.7 Inhibition of T cell proliferation assay

The standardized Mye-EUNITER protocol was used¹²². At day 0, CD14 monocytes were isolated from healthy donor PBMC and stimulated for 24 h with 2 µg/mL rHSP90α. At day 1, CD3 T cells were isolated with human anti-CD3 magnetic beads (Miltenyi Biotec) from PBMC of another healthy donor and labelled with 20 µM cell proliferation dye eFluor 450 (CPDye405, eBioscience) according to manufacturer's instructions. For the stimulation of T cells, a 96-well cell culture plate (Sarstedt) was coated for 2 h at 37°C with human anti-CD3 (1 µg/ml, clone OKT-3, eBioscience) and human anti-CD28 antibodies (2 µg/ml, clone CD28.2, Beckman Coulter). Monocytes, stimulated for 24 h, were washed and transferred on the pre-coated plate for 96-hour co-culture with T cells in Low Arginine medium (Table 4). After 96 hours, the proliferation of T cells was detected by measuring proliferation dye dilution on FACS Lyric (BD Biosciences) flow cytometer.

4.2.8 Transwell migration assay

HT144 melanoma cells were grown confluent in full RPMI medium, washed with PBS and resuspended in serum-free RPMI medium. To the well of the 24-well plate full or serum-free RPMI medium was added supplemented with different concentrations of rHSP90 α . Full or serum-free RPMI medium supplemented with different concentrations of rHSP90 α was pipetted to wells of the 24-well plate. 0.4 μ m inserts were positioned in the wells, with the bottom of the insert merged in medium. 2×10^5 cells in 200 μ L were added to the upper compartment of each insert. Plate was incubated for 24 h at 37°C. Next, the inserts were taken out carefully and were transferred into wells filled with 500 μ L methanol and 100 μ L methanol added in the upper compartment for cell fixation. Cells were fixed for 10 min at room temperature and then the fluid was removed. For the staining, cells were incubated with 1% crystal violet in 2% ethanol for additional 20 min. The inserts were washed with PBS to remove excess dye. Cells in the upper compartment of the insert were removed by gently wiping the upper side of the membrane with a cotton swab. Bottom of each transwell was cut with a scalpel and transferred into a 96-well flat bottom plate filled with 0.1% SDS in order to dissolve the dye. Optical density was then measured photometrically at 570 nm. The relative migration was calculated according to the migration level of untreated cells incubated in serum-free medium.

For human monocytes, 2×10^5 cells were seeded into the upper compartment of each insert installed as described above. After the 24 h incubation at 37°C, inserts were discarded, cells remaining in the wells were collected, washed with PBS and counted at flow cytometer.

4.2.9 Patients

We selected 44 patients with stage III–IV melanoma who did not receive any systemic therapy at least for 3 months before their enrollment. The patients were treated with ICI (nivolumab or pembrolizumab as a monotherapy or nivolumab in combination with ipilimumab) or received targeted therapy (dabrafenib and trametinib or binimetinib). Peripheral

blood samples were collected after written informed consent. For the patients who received ICIs, response to the treatment was assessed according to the Immunotherapy Response Evaluation Criteria in Solid Tumours (iRECIST) 12 weeks after the first administration of ICI. Based on the response, patients were divided into responders showing complete response, partial response or mixed response and non-responders (progressive disease).

4.2.10 Statistical analysis

Data were statistically analyzed using the GraphPad Prism software. For the analysis were taken experiments with at least three biological replicates (different healthy donors or patients, independent experiments for the cell line). The two-tailed Student's t test was used for the normally distributed data and for the Mann-Whitney test for not normally distributed data. Generation of the survival curves was done by the Kaplan-Meier method and the log rank (Mantel-Cox) test was used for the comparison. Data are presented as mean \pm standard deviation. Differences were considered significant if * $p \leq 0.05$, ** $p \leq 0.01$ and *** $p \leq 0.001$.

5 RESULTS

5.1 Expression and purification of the recombinant (r) HSP90 α

In order to investigate the capacity of the soluble HSP90 α to convert myeloid cell into immunosuppressive ones, we treated normal human monocytes with rHSP90 α and check whether it can upregulate immunosuppressive molecule PD-L1 on their surface. The analysis was performed by flow cytometry and the gating strategy is displayed in the Figure 4A. We tested several commercially available rHSP90 α , expressed either in *E. coli* or in baculovirus-transfected insect cells, and observed a strong upregulation of the PD-L1 after 16 h of stimulation (Fig.4B). Since rHSP90 α is a putative TLR4 ligand, it would be important to test a possible lipopolysaccharide (LPS) contamination that could cause the PD-L1 upregulation. Giving that LPS is heat-intact, we boiled the solution at 95°C for 10 min, then tested the ability to stimulate monocytes and found that the PD-L1 upregulation still occurred (except for the Source 2 Lot 1 that was not available for further purchase) (Fig.4B), indicating a high LPS contamination. Therefore, we decided to perform the expression and purification of rHSP90 α in our laboratory, including an additional washing step with Triton-X 114 for removing LPS.

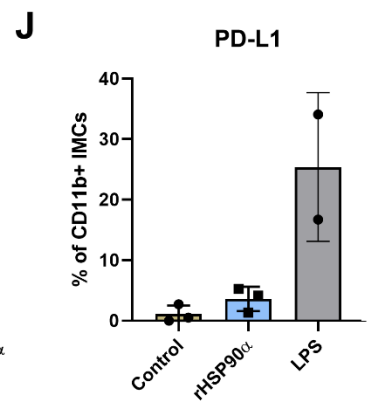
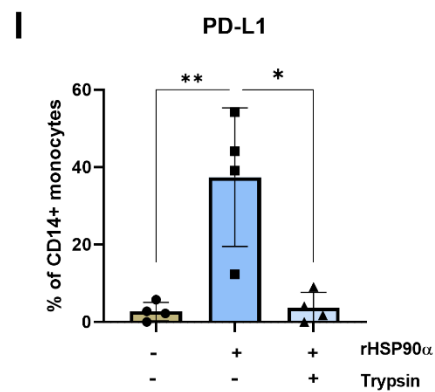
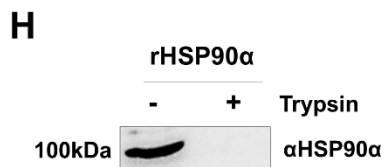
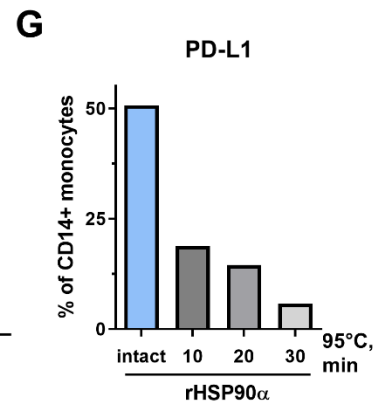
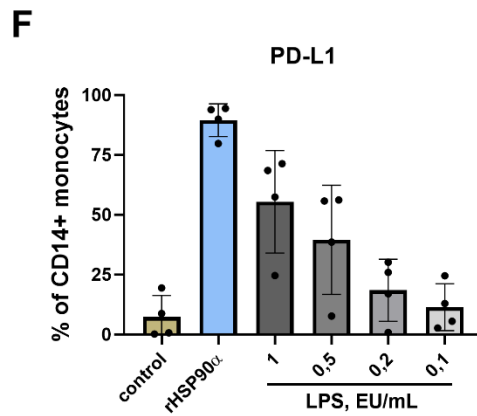
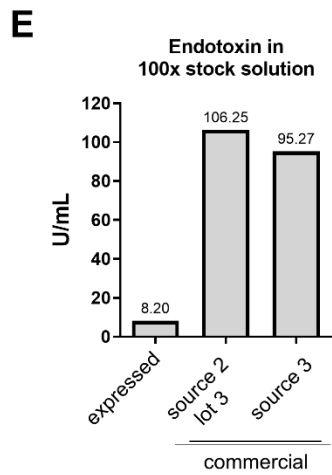
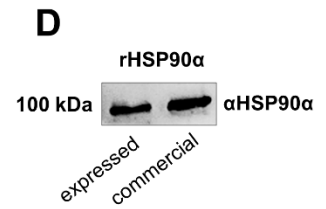
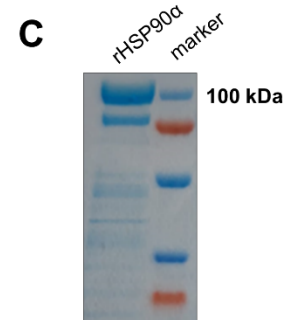
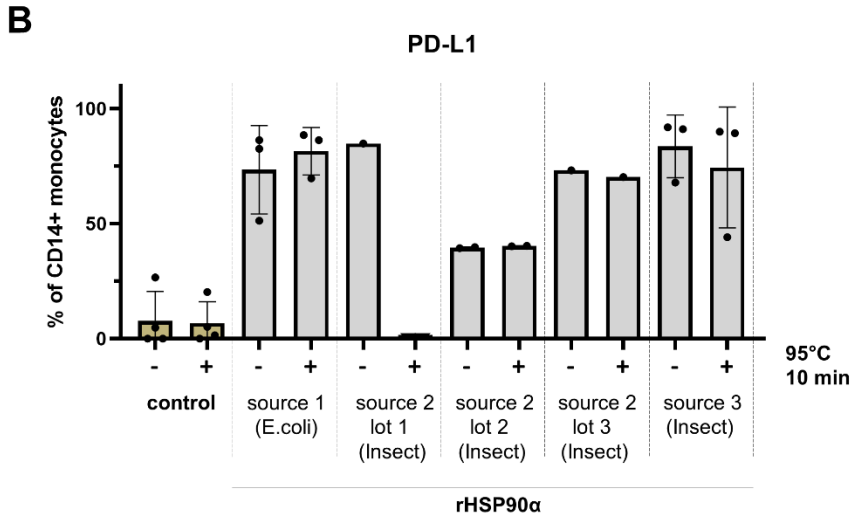
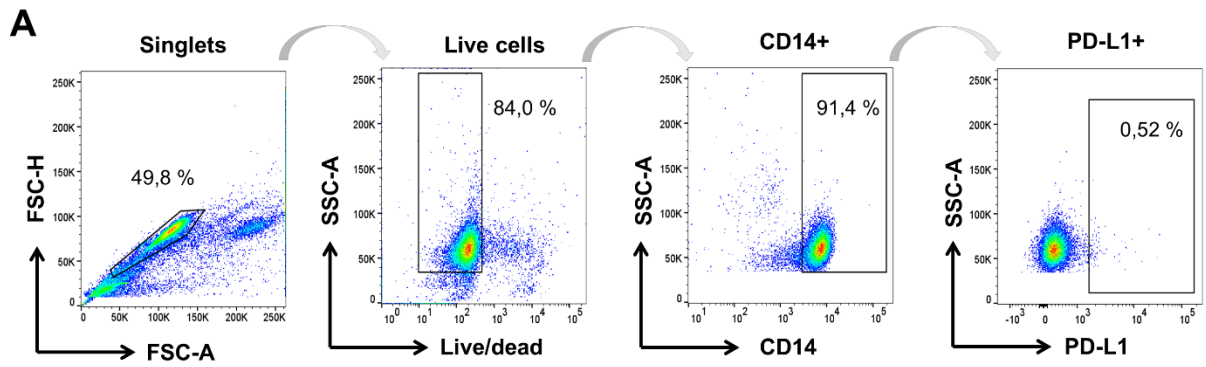


Figure 4. Expression and purification of the rHSP90 α . (A) Gating strategy for the surface marker expression on monocytes. Representative dot plots are shown for freshly isolated human CD14 monocytes. Monocytes were gated after exclusion of doublets and dead cells. (B) Induction of PD-L1 on human monocytes by rHSP90 α from different manufacturers. Human monocytes were treated with 2 μ g/mL rHSP90 α or PBS (control) for 16 h *in vitro*. The expression of PD-L1 was analyzed by flow cytometry, n=1-4. (C) Coomassie staining of the internally expressed and purified rHSP90 α . (D) Western blot analysis of the internally expressed and purified rHSP90 α . (E) Endotoxin measurement in the different rHSP90 α preparations. Measurement was performed by Limulus Amebocyte Lysate assay, n=1. (F) PD-L1 expression on human monocytes upon treatment with lipopolysaccharide (LPS), n=4. (G) Heat-inactivation of the rHSP α , n=1. (H) Digestion of rHSP90 α with trypsin. rHSP90 α was incubated with immobilized trypsin for 18 h at 37°C. Then trypsin-beads were pelleted, and the supernatant was tested by Western Blot. (I) PD-L1 expression on human monocytes stimulated with Trypsin-digested rHSP90 α , n=4. (J) PD-L1 expression on mouse immature myeloid cells (IMC) stimulated with rHSP90 α or 100 EU/mL LPS, n=2-3. Results on the graphs B, F, G, I, J (mean \pm SD) are presented as the percentage of PD-L1⁺ monocytes among total monocytes or IMC. *p < 0.05, **p < 0.01. Coomassie staining was performed by Daniel Novak PhD. IMC isolated by Samantha Lasser.

Expression of the rHSP90 α was confirmed by Coomassie staining (Fig.4C) and Western Blot (Fig.4D). Noticeably, we observed a fraction of the recombinant protein having molecular weight of around 70 kDa, indicating a possible proteolytic degradation. LPS concentration in the final preparation of the rHSP90 α was measured by Limulus Amebocyte Lysate assay and found to be as low as 8.2 EU/mL for 100x stock solution that corresponds to 4.3 mEU/mL as a final concentration (Fig.4E) and is not enough to upregulate PD-L1 (Fig.4F). The same heating test as for the commercial proteins (95°C for 10 minutes or longer) demonstrated the

disappearance of the PD-L1 upregulation, suggesting that the observed effect was protein-mediated (Fig.4G). For further proof that PD-L1 upregulation was mediated by rHSP90 α and not contaminating LPS, we carried out digestion with bead-immobilized trypsin. Such treatment led to the complete disappearance of rHSP90 α (Fig.4H) that was associated with the abrogated PD-L1 upregulation (Fig.4I). Moreover, rHSP90 α failed to upregulate PD-L1 in mouse immature myeloid cells (IMC) (Fig.4J) indicating specificity of the protein-mediated effect to human while LPS contamination would have cross-species reactivity.

5.2 Recombinant HSP90 α triggers TLR4 signaling in human monocytes to induce PD-L1 expression

Collective data of PD-L1 expression on human monocytes from different experiments demonstrates consistent upregulation of PD-L1 by rHSP90 α although with a broad distribution of a magnitude of the upregulation, which could be due to the individual reactivity of healthy donors (Fig.5A). Since it was previously demonstrated that melanoma-derived EV induced immunosuppressive myeloid cells mainly via TLR4, but also via TLR2³⁹, we further studied if TLR4 or TLR2 could be responsible for rHSP90 α -mediated PD-L1 upregulation. We found that blocking anti-TLR4 mAbs abrogated the upregulation of PD-L1 expression (Fig.5B). In contrast, blocking anti-TLR2 mAbs or isotype control mAbs failed to mediate such blockade, indicating that rHSP90 α indeed binds to TLR4. We then tested if NF- κ B was involved in PD-L1 upregulation as a transcription factor downstream of TLR4. The NF- κ B inhibitor Bay 11-7082 (Bay) was checked for its cytotoxic activity and titrated in apoptosis assay. We found that 2 μ M of Bay did not affect monocyte viability and used this concentration for further experiments (Fig.5C). The addition of Bay blocked the upregulation of PD-L1 by rHSP90 α (Fig.5D). Activation of NF- κ B was confirmed by increased phosphorylation of the p65 by Western Blot (Fig.5E). Bitsch et al. have demonstrated an importance of STAT3 activation for

the generation of MDSC⁶³. Therefore, we tested the phosphorylation of STAT3 and found its increase under the treatment with rHSP90 α (Fig.5E).

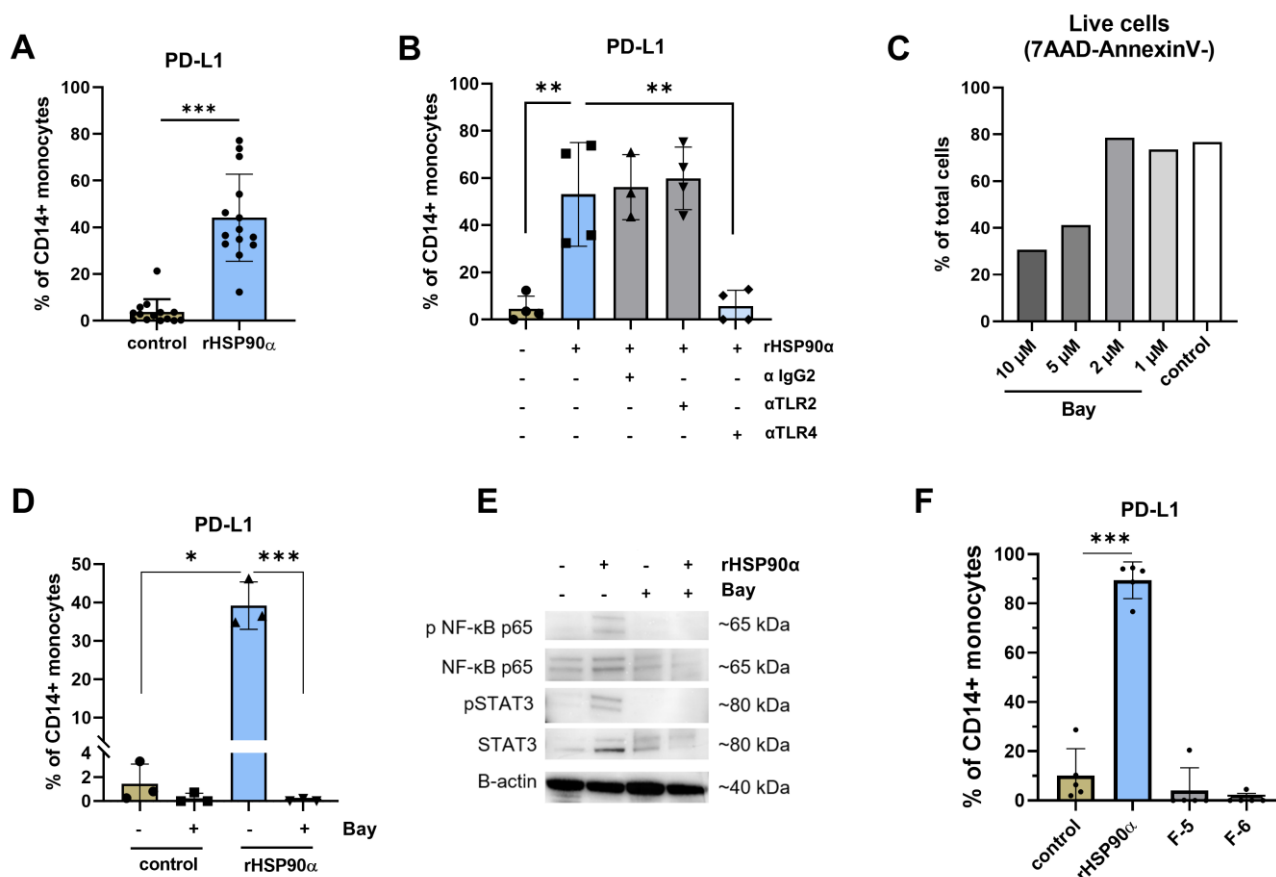


Figure 5. Induction of PD-L1 on human monocytes by rHSP90 α is dependent on the TLR4-NF- κ B signaling. (A) Human monocytes were treated with 2 μ g/mL/10⁶ cells rHSP90 α or PBS (control) for 16 h *in vitro* (n=14). The expression of PD-L1 was analyzed by flow cytometry. (B) Monocytes were treated with rHSP90 α in the presence of anti-TLR2 or anti-TLR4 mAbs (n=3-4). (C) Monocytes were treated with different concentrations of NF- κ B inhibitor Bay (n=1). Percentage of live cells (7-AAD⁻AnnexinV⁻) was analyzed by flow cytometry. (D) Monocytes were stimulated with rHSP90 α in the presence of Bay (n=3). (E) Expression of NF- κ B and STAT3 in monocytes treated with rHSP90 α in the presence or absence of Bay was analyzed by Western Blot. (F) PD-L1 expression on monocytes stimulated with F-5 and F-6 subfragments of HSP90 α for 16 h (n=4). Results on the graphs A,B, D, and F

(mean \pm SD) are presented as the percentage of PD-L1⁺ monocytes among total monocytes. * $p < 0.05$, ** $p < 0.01$, *** $p < 0.001$. Western Blot performed in collaboration with Laura Hüser PhD.

It was shown that central M domain of HSP90 α was responsible for protumoral effects of soluble HSP90 α and its interaction with the low-density lipoprotein receptor-related protein-1 (LRP1 or CD91)¹⁰⁷ suggesting an alternative receptor for rHSP90 α since LRP1 is abundantly expressed on monocytes¹²³. Therefore, we purified F-5 and F-6 subfragments of HSP90 α that contain a key amino acid sequence of central M domain of HSP90 α responsible for the binding to LRP1¹⁰⁷. Both fragments failed to induce PD-L1 expression in human monocytes when tested at the same concentrations as full rHSP90 α (Fig.5F).

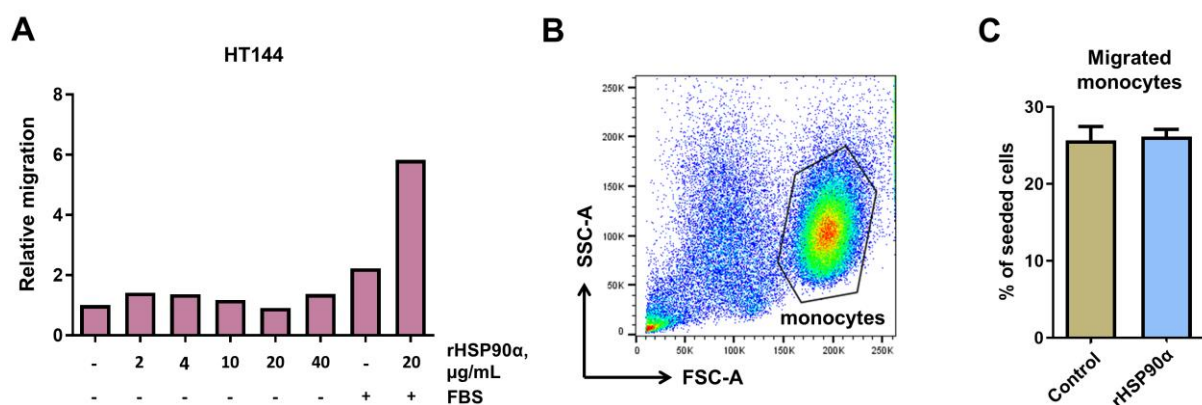


Figure 6. Cell migration upon rHSP90 α treatment. (A) Migration of HT144 melanoma cell upon the treatment with different concentrations of rHSP90 α in the presence or absence of FBS (n=1). (B) Representative dot plot showing gating according to monocyte morphology. (C) Proportion of migrated monocytes upon the treatment with 2 μ g/mL of rHSP90 α calculated according to the number of seeded cells (n=3, mean \pm SD).

Zou et al. demonstrated that HSP90 α binding to LRP1 leads to an increased motility of tumor cells¹⁰⁷. We confirmed this pro-motility effect for melanoma cell line HT144 in a

transwell migration assay (Fig.6A). To test whether HSP90 α could induce such effect for monocytes, we performed a trans-well migration assay quantifying the migrated cells via flow cytometry (Fig.6B). However, we failed to detect any increase in the migration capacity of rHSP90-treated monocytes (Fig.6C).

Collectively, our data suggested that soluble rHSP90 α similar to exosomal HSP90 α could trigger PD-L1 upregulation in human monocytes via TLR4 signaling.

5.3 Recombinant HSP90 α converts human monocytes into immunosuppressive MDSC and rescues them from apoptosis via TLR4 signaling

Since it was described that human M-MDSC differ from monocytes due to downregulated Human Leukocyte Antigen DR (HLA-DR) expression²⁵ we studied the kinetics of HLA-DR expression by flow cytometry in rHSP90 α -treated and untreated monocytes. We observed a slight initial upregulation of HLA-DR at 16 h followed by downregulation at 24 h of treatment (Fig.7A, B).

Alongside HLA-DR downregulation, we observed a retained expression of the monocytes marker CD14 in treated monocytes while untreated cells were losing this receptor (Fig.7C) that could be linked to cells viability. In order to clarify this finding, we performed an apoptosis assay with Annexin V and 7-AAD staining. In this assay, Annexin V and 7-AAD double negative population indicates viable cells, Annexin V positive 7-AAD negative population – early apoptotic cells, Annexin V and 7-AAD double positive population – late apoptotic cells (Fig.7D). Indeed, rHSP90 α treatment could rescue monocytes from apoptosis in TLR4- and NF- κ B-dependent manner (Fig. 7E,F). Abovementioned CD14 retention effect was observed in viable cell population but not in apoptotic cells (Fig.7G), providing an explanation of this phenomenon.

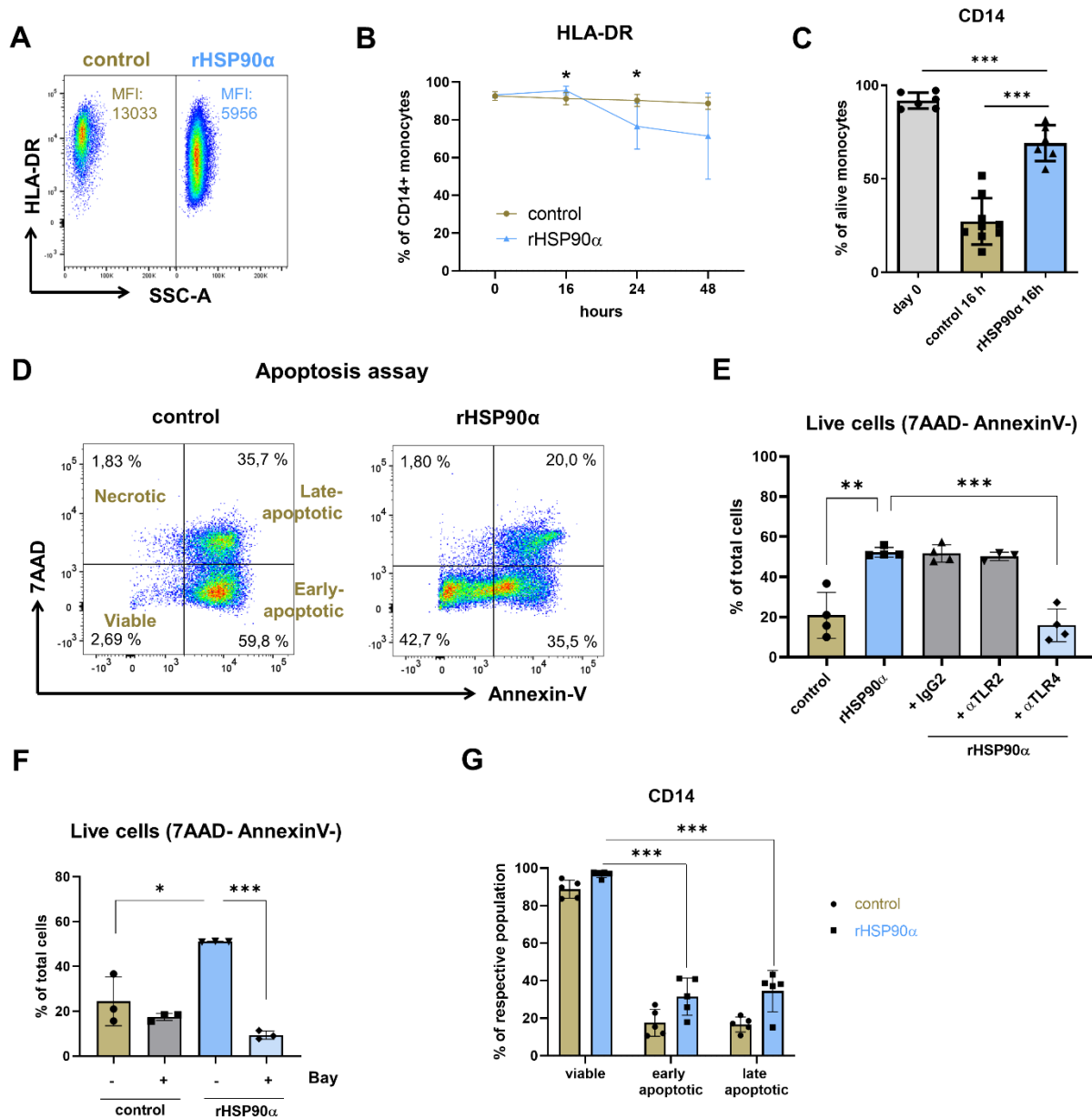


Figure 7. Phenotype and viability changes in monocytes upon rHSP90 α treatment. (A) Representative dot plot showing HLA-DR expression on CD14 monocytes upon 24 h of treatment with rHSP90 α . (B) HLA-DR expression on rHSP90 α -treated monocytes was shown as the percentage of HLA-DR⁺ cells among total monocytes (mean \pm SD; n=5). (C) CD14 expression on monocytes after the isolation and after 16 h stimulation with rHSP90 α . Data shown as the percentage of live cells (mean \pm SD; n=6-9). (D) Gating strategy for apoptosis of

monocytes treated with rHSP90 α for 24 h. Dot plots show Annexin V⁻7-AAD⁻ live cells, Annexin V⁺7-AAD⁻ early apoptotic cells, and Annexin V⁺7-AAD⁺ late apoptotic cells. (E) Human monocytes were treated for 24 h with PBS (control) or 2 μ g/mL rHSP90 α alone or in the presence of anti-TLR2 or anti-TLR4 mAbs. Apoptosis of monocytes was measured by flow cytometry. Data are presented as the percentage of live (Annexin V⁻7-AAD⁻) cells among total monocytes (mean \pm SD; n=3-4). (F) Monocytes were treated with rHSP90 α alone or together with the NF- κ B inhibitor Bay. Results are presented as the percentage of live (Annexin V⁻7-AAD⁻) cells within total monocytes (mean \pm SD; n=3). (G) CD14 expression was measured on viable, early and late apoptotic monocytes. Data are presented as the percentage of a respective population (mean \pm SD; n=5). *p < 0.05, **p < 0.01, ***p < 0.001.

To study which mechanisms underlie the rHSP90 α -mediated survival effect, we measured the RNA expression by RT-PCR of several pro- and anti-apoptotic genes, namely caspase 3, BCL2 associated X (BAX), myeloid cell leukemia sequence 1 (MCL 1), and B-cell lymphoma 2 (BCL 2). After 24 h of stimulation we did not observe any significant changes in the expression of abovementioned genes (Fig.8A-D).

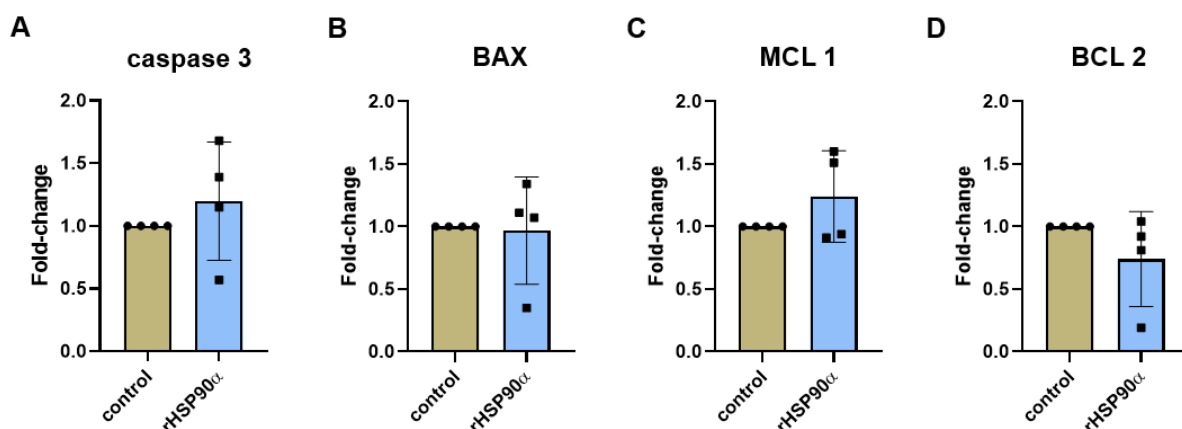


Figure 8. Expression of pro- and anti-apoptotic genes in rHSP90 α -treated monocytes. mRNA expression of caspase 3 (A), BAX (B), MCL 1 (C), and BCL 2 (D) genes was measured

by qRT-PCR. Values were normalized for the housekeeping gene Rn18s expression and the unstimulated control according to the $2^{-\Delta\Delta CT}$ method (mean \pm SEM; n=4).

Next, we performed inhibition of T cell proliferation assay, co-culturing activated CD3 T cells with rHSP90 α -treated monocytes in the 1:2 ratio. Cells that were losing cell proliferation dye staining were gated as proliferated ones (Fig.9A). We observed that rHSP90 α -treated monocytes could inhibit proliferation of T cells compared to untreated monocytes and to T cells cultured alone (Fig.9B, C).

These findings indicate that soluble HSP90 α can not only endow monocytes with phenotype and function of MDSC but also prolong their survival.

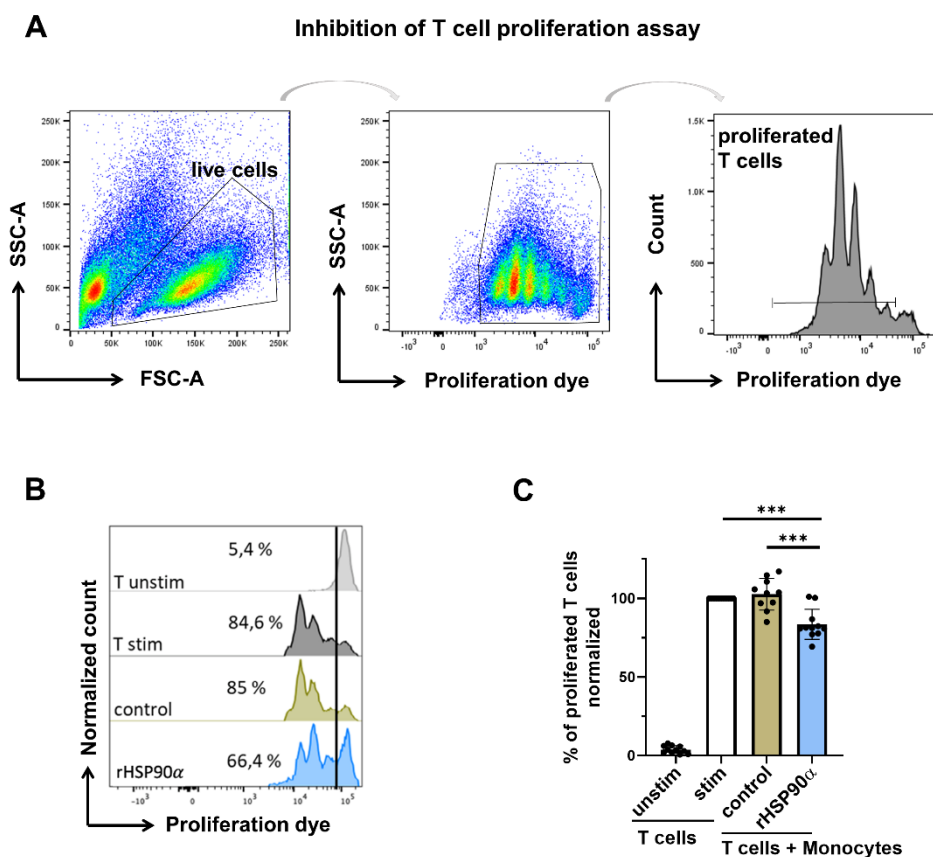


Figure 9. Suppressive capacity of rHSP90 α -treated monocytes. (A) Gating strategy for proliferated T cells stimulated for 96 h. **(B)** Representative histograms for proliferated T cells

cultured for 96 h alone or together with non-treated (control) monocytes or cells treated with 2µg/mL rHSP90α. (C) Cumulative data for T cell proliferation are presented as the percentage of divided T cells normalized (norm.) to the respective control of stimulated T cells alone (mean ± SD; n=11). ***p < 0.001. Inhibition of T cell proliferation performed in collaboration with Feyza Gül Özbay Kurt.

5.4 rHSP90α-treated monocytes acquired immunosuppressive capacity via TLR4-dependent upregulation of PD-L1

MDSC exploit a broad variety of immunosuppressive mechanism for hindering the antitumor immune response⁴⁷. Therefore, we tested which other immunosuppressive markers, except PD-L1, might be induced on human monocytes by the treatment with rHSP90α, including increased production of ROS and NO as well as elevated expression of Arg-1 and ectonucleotidases CD39 and CD73⁴⁷. However, no significant changes between treated and non-treated monocytes were detected (Fig. 10A-G). When adding blocking anti-PD-L1 antibodies to the co-culture of rHSP90α-treated monocytes and T cells, we found a significant reduction of monocyte immunosuppressive activity (Fig.11A, B). However, this downregulation was not complete, suggesting possible additional mechanisms of immunosuppression.

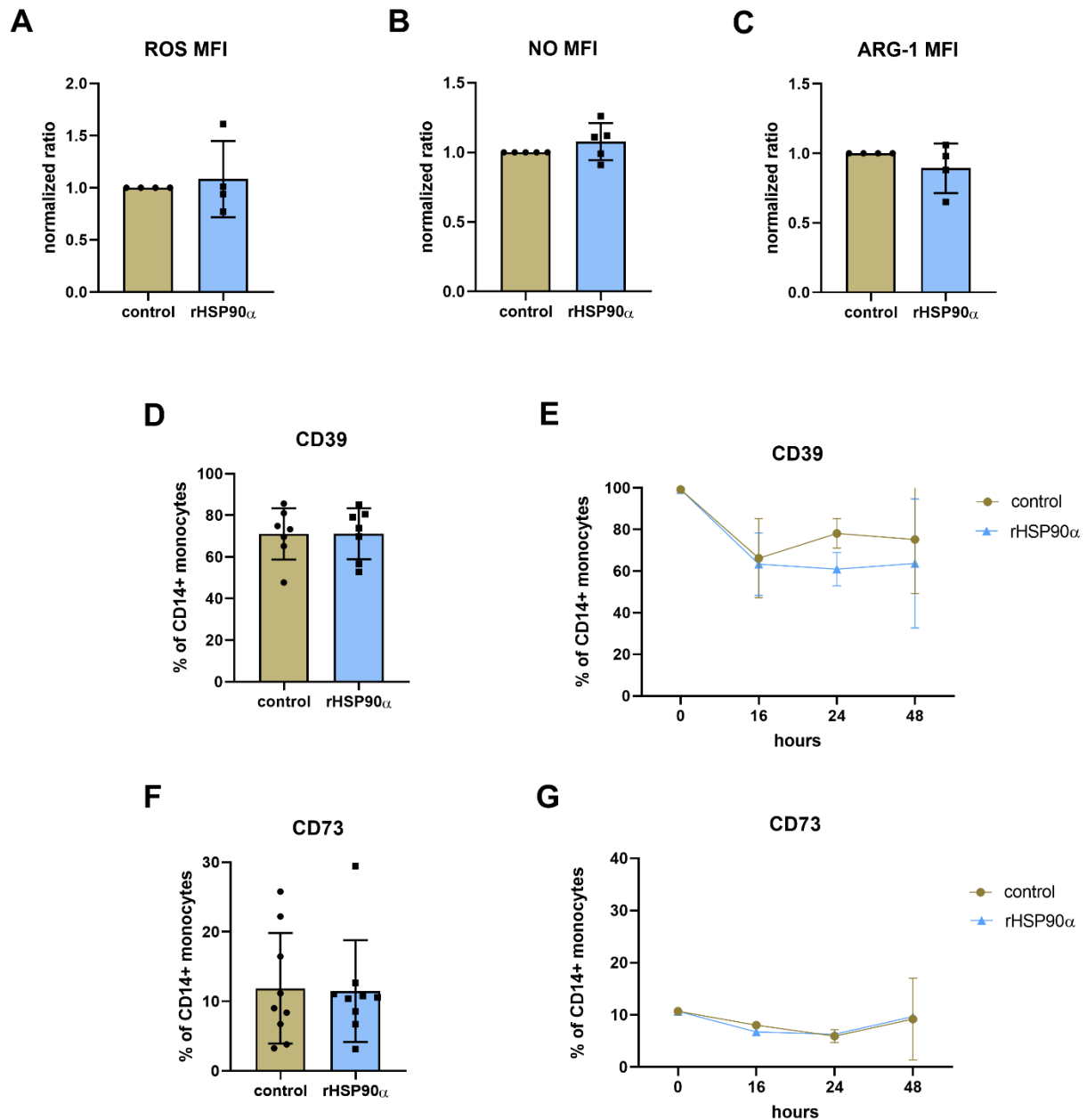


Figure 10. Effect of rHSP90 α on production of ROS and NO as well as expression of Arg-1, CD39 and CD73 in monocytes. Monocytes were treated with 2 μ g/mL rHSP90 α or PBS (control). Production of ROS (A), NO (B) and expression of ARG-1 (C) is presented as normalized mean fluorescence intensity (MFI) (mean \pm SD; n=4). Expression of CD39 (D, E), and CD73 (F,G) is shown as the percentage of CD39⁺ or CD73⁺ monocytes among total monocytes (mean \pm SD; n=3-9).

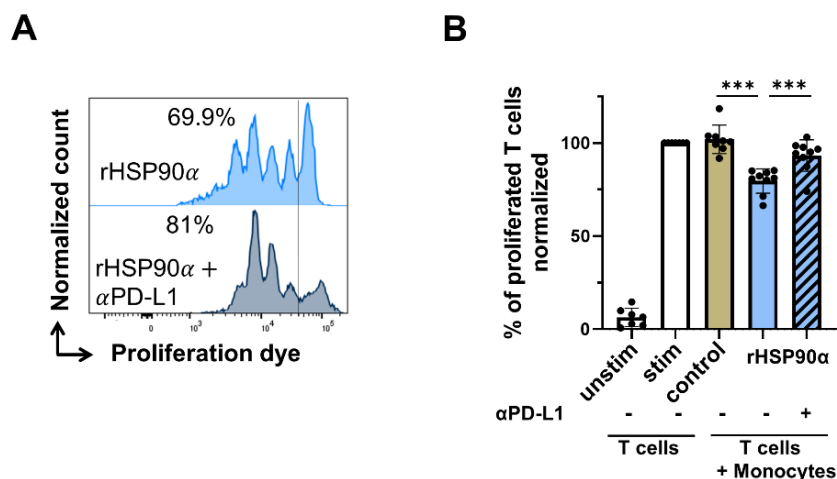


Figure 11. Role of PD-L1 expression in immunosuppressive capacity of rHSP90 α -treated monocytes. (A) Representative histograms for proliferated T cells co-cultured with rHSP90 α -treated monocytes with or without blocking anti-PD-L1 mAbs. (B) Cumulative data for T cell proliferation co-cultured with rHSP90 α -treated monocytes and anti-PD-L1 mAbs. Data are shown as the percentage of divided T cells normalized (norm.) to the respective control of stimulated T cells alone (mean \pm SD; n=7-9). **p < 0.01, ***p < 0.001. Inhibition of T cell proliferation performed in collaboration with Feyza Gül Özbay Kurt.

5.5 Expression of MDSC-related genes in rHSP90 α -stimulated monocytes

To shed more light into possible additional mechanisms of immunosuppression and into the anti-apoptotic effects of rHSP90 α , we performed microarray analysis comparing rHSP90 α -treated and non-treated (control) monocytes. Gene expression profiling confirmed the elevated expression of PD-L1 (*CD274*) (Fig.9A). In addition, several MDSC-related genes including *IDO-1*, *CCL2*, and *CXCL5*, were elevated (Fig.12A). Among the genes important for the immunostimulatory function of myeloid cells, *CD38* and *CD80* were slightly upregulated whereas *CD86* was downregulated (Fig.12A). Pathway analysis revealed upregulated expression of genes related to oxidative phosphorylation, IL-1 signalling, antigen processing

etc. in HSP90 α -treated monocytes (Fig.12B). The microarray data generated during the study is made available on the GEO repository under the number GSE207075.

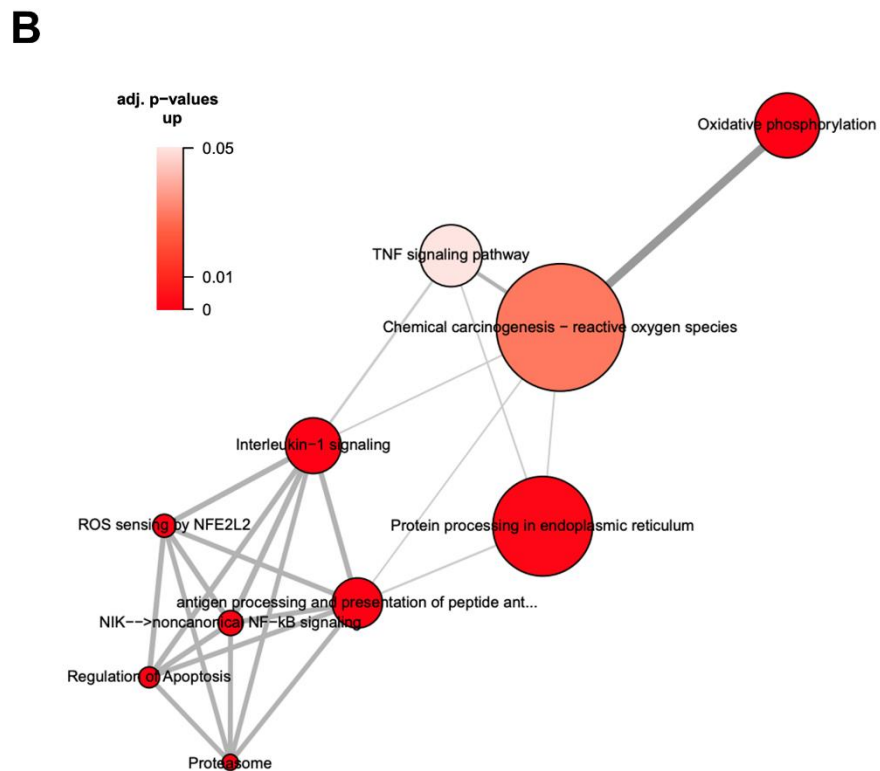
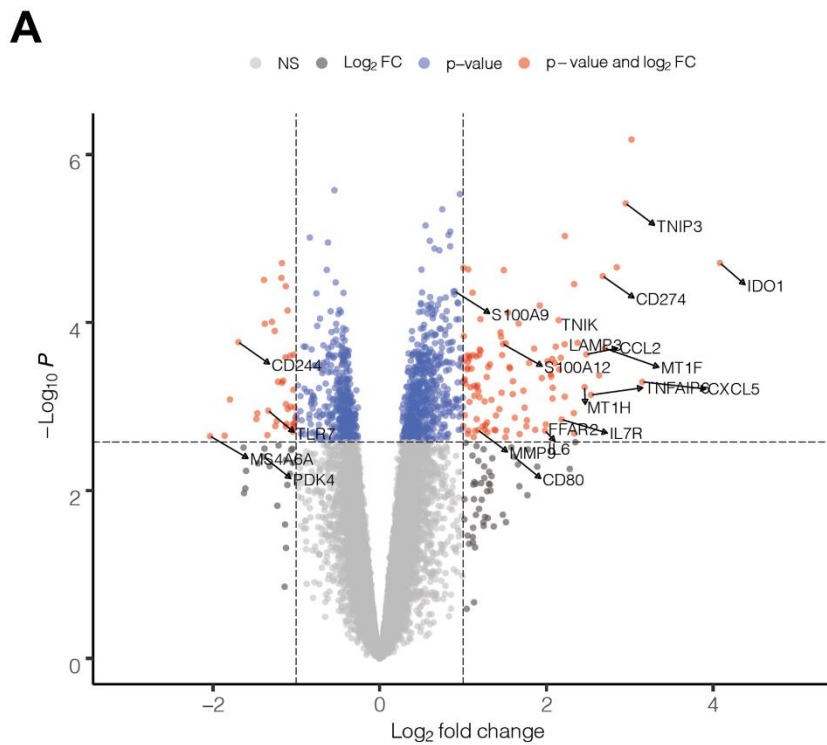


Figure 12. Microarray analysis of rHSP90 α -treated monocytes. Transcriptome of monocytes treated for 24 h with 2 μ g/mL rHSP90 α vs. non-treated monocytes (n=4) (A) Volcano plot representing differentially expressed genes. Arrows indicate selected differentially regulated genes. Horizontal dashed line indicates the significance threshold ($p < 0.05$). Vertical dashed line indicates 2-fold change. (B) Enrichment map representing selected upregulated pathways in rHSP90 α -treated vs. untreated monocytes. Intensity of the red color indicates significance and the size of the circle indicates the number of genes. The line thickness indicates the number of overlapping genes. Microarray analysis performed in collaboration with Feyza Gül Özbay Kurt and Thomas Hielscher PhD.

5.6 TLR4-NF- κ B-dependent upregulation of IDO-1 endows rHSP90 α -treated monocytes with immunosuppressive capacity

The finding of *IDO1* gene upregulation by the microarray analysis indicated that IDO1, in addition to PD-L1, might contribute to the immunosuppressive capacity of rHSP90 α -treated monocytes and explain the remaining suppression upon the treatment with blocking anti-PD-L1 antibodies (Fig.11A, B). Upregulation of IDO1 at the protein level in human monocytes upon 16 h of treatment was confirmed by Western Blot and, similarly to PD-L1, was demonstrated to be NF- κ B and TLR4-dependent (Fig.13A). The Addition of the IDO1 inhibitor 1-methyl-D-tryptophan (1-D-MT) blocked the immunosuppressive activity of rHSP90 α -treated monocytes in the co-culture with T cells (Fig.13B, C).

In order to verify a synergistic effect of PD-L1 and IDO1 blockade, we performed a separate set of experiments co-culturing rHSP90 α -treated monocytes and T cells in the presence of anti-PD-L1 antibody and 1-D-MT alone or both agents together. No significant difference was observed between anti-PD-L1 or anti-IDO1 monotherapy as compared to the combinational treatment (Fig.13F, G) suggesting no additive effect. Interestingly, monocytes

from two healthy donors showed different reaction to these blocking agents (Fig.13G). In one (green dots on the graph), only anti-PD-L1 blockade was effective to restore T cell proliferation and not the 1-D-MT. In another one (red dots on the graph), only 1-D-MT was effective and not the anti-PD-L1 blocking antibody. Inhibition of T cell proliferation performed in collaboration with Feyza Gül Özbay Kurt.

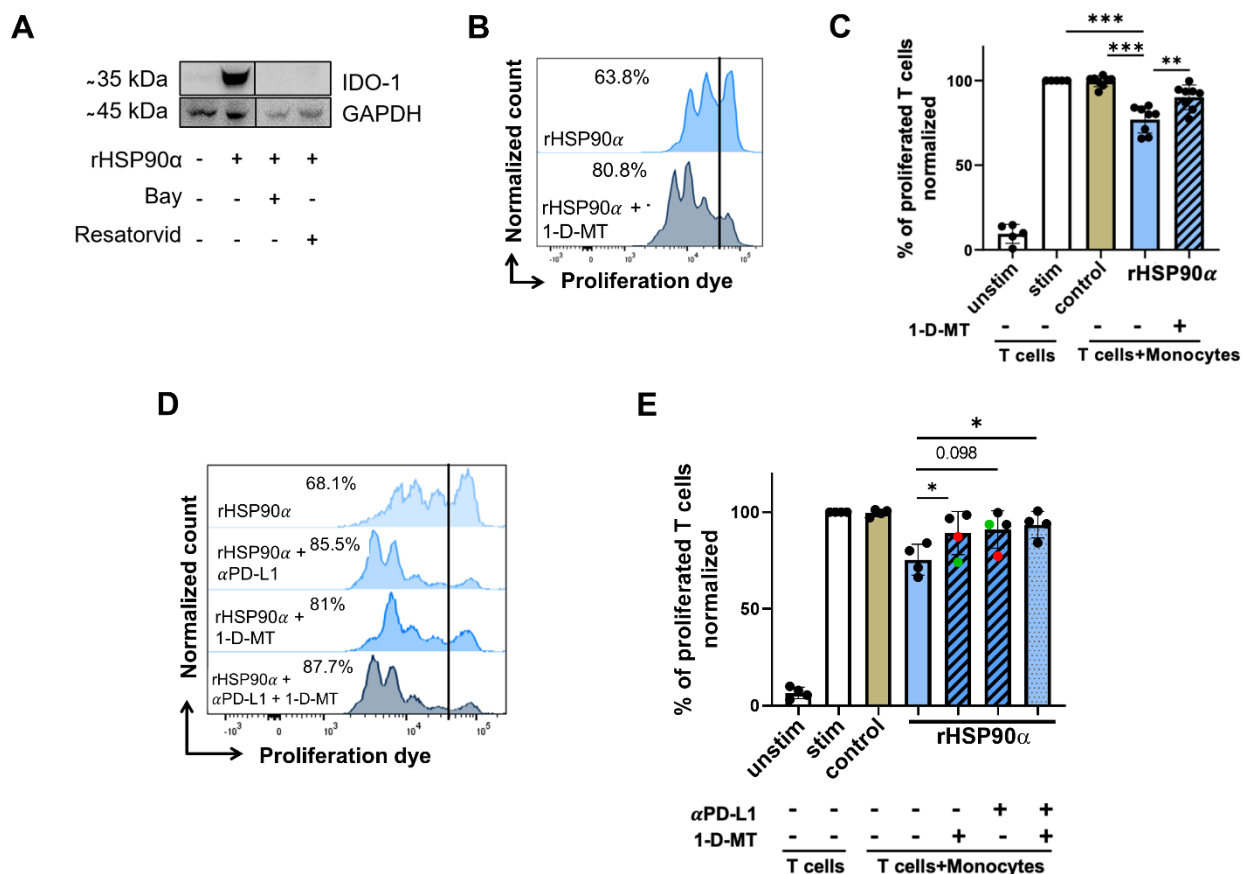


Figure 13. Impact of IDO-1 on immunosuppressive activity of rHSP90α-treated monocytes.

(A) Expression of IDO-1 in monocytes treated with 2μg/mL rHSP90α was measured by Western Blot. The representative experiment out of three is shown. (B) Representative histograms for proliferated T cells co-cultured with rHSP90α-treated monocytes with or without the IDO-1 inhibitor 1-D-MT. (C) Cumulative data for T cell proliferation co-cultured with rHSP90α-treated monocytes and 1-D-MT. Data are shown as the percentage of divided T cells normalized (norm.) to the respective control of stimulated T cells alone (mean ± SD; n=5-8). (D) Representative

histograms for proliferated T cells co-cultured with rHSP90 α -treated monocytes alone or together with anti-PD-L1 mAbs and/or 1-D-MT. **(E)** Cumulative data for T cell proliferation co-cultured with rHSP90 α -treated monocytes together with anti-PD-L1 mAb and/or 1-D-MT 1-D-MT. Results are presented as the percentage of divided T cells normalized (norm.) to the respective control of stimulated T cells alone (mean \pm SD; n=4). *p < 0.05 , **p < 0.01, ***p < 0.001.

5.7 HSP90 α in plasma of melanoma patients

To investigate an impact of soluble HSP90 α on myeloid cells in advanced melanoma patients, we measured the frequency of circulating M-MDSC and monocytes and their PD-L1 expression as well as the HSP90 α concentration in plasma from the same patients by ELISA. Since EV can also contain HSP90 α ³⁹, we first tested if the ELISA kit could detect only soluble or also EV-derived HSP90 α . For this, we depleted EV by ultracentrifugation of plasma samples from melanoma patients at 100,000 g for 16 h and found no significant differences in HSP90 α concentrations between whole and EV-depleted samples, indicating that the ELISA kit detects only soluble HSP90 α and that HSP90 α is present in plasma mostly as a soluble protein (Fig. 14).

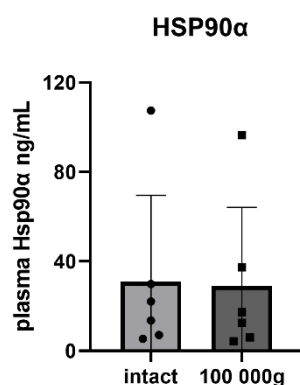


Figure 14. Impact of ultracentrifugation on the level of HSP90 α in plasma of melanoma patients. Concentration of HSP90 α was measured by ELISA in plasma before or after the ultracentrifugation at 100,000 g for 16 h. Data are presented as ng/mL.

Gating strategy for the surface marker analysis in human circulating myeloid cells and cell sorting are shown in Fig. 15A. We observed a tendency for the correlation between decreased monocyte frequencies and increased HSP90 α plasma levels (Fig. 15B). An elevated

PD-L1 expression on circulating M-MDSC showed a significant correlation with an increased concentration of HSP90 α (Fig. 15C).

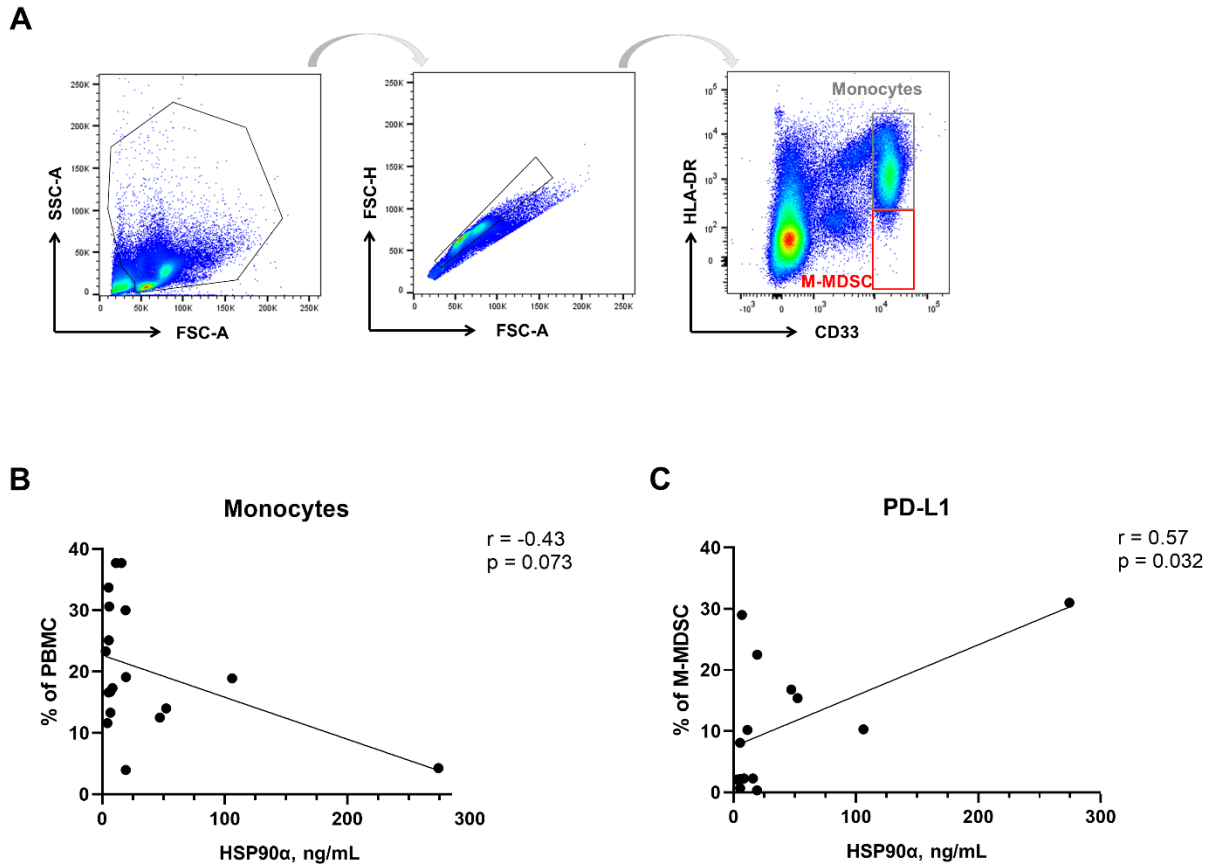


Figure 15. Effect of soluble HSP90 α on myeloid cells in melanoma patients. Monocytes and M-MDSC were sorted from the PBMC of melanoma patients at the baseline and during the therapy and analyzed by flow cytometry. (A) Gating strategy for sorting of monocytes and M-MDSC via FACS. After exclusion of cell debris and doublets, monocytes and M-MDSC were sorted from PBMC according to the expression of HLA-DR and CD33. The concentration of HSP90 α was detected in plasma of the same patients by ELISA. The frequency CD14 monocytes within PBMC (B; n=18) or PD-L1⁺ M-MDSC among total MDSC (A; n=14) were plotted against the levels of HSP90 α expressed in ng/mL. The correlation was evaluated by a

linear regression analysis. ELISA and FACS staining was performed in collaboration with Rebekka Bitsch and Feyza Gül Özbay Kurt.

Finally, we investigated the impact of soluble HSP90 α levels on the clinical outcome of melanoma patients treated with ICI. The concentration of HSP90 α was measured in plasma before treatment initiation. We found a strong tendency for the prolonged PFS in patients with lower concentrations of HSP90 α (Fig. 16A), whereas OS was similar in patients with higher and lower levels of HSP90 α (Fig. 16B). Furthermore, patients responding to the ICI treatment tended to have lower plasma levels of HSP90 α before the onset of therapy (Fig. 16C).

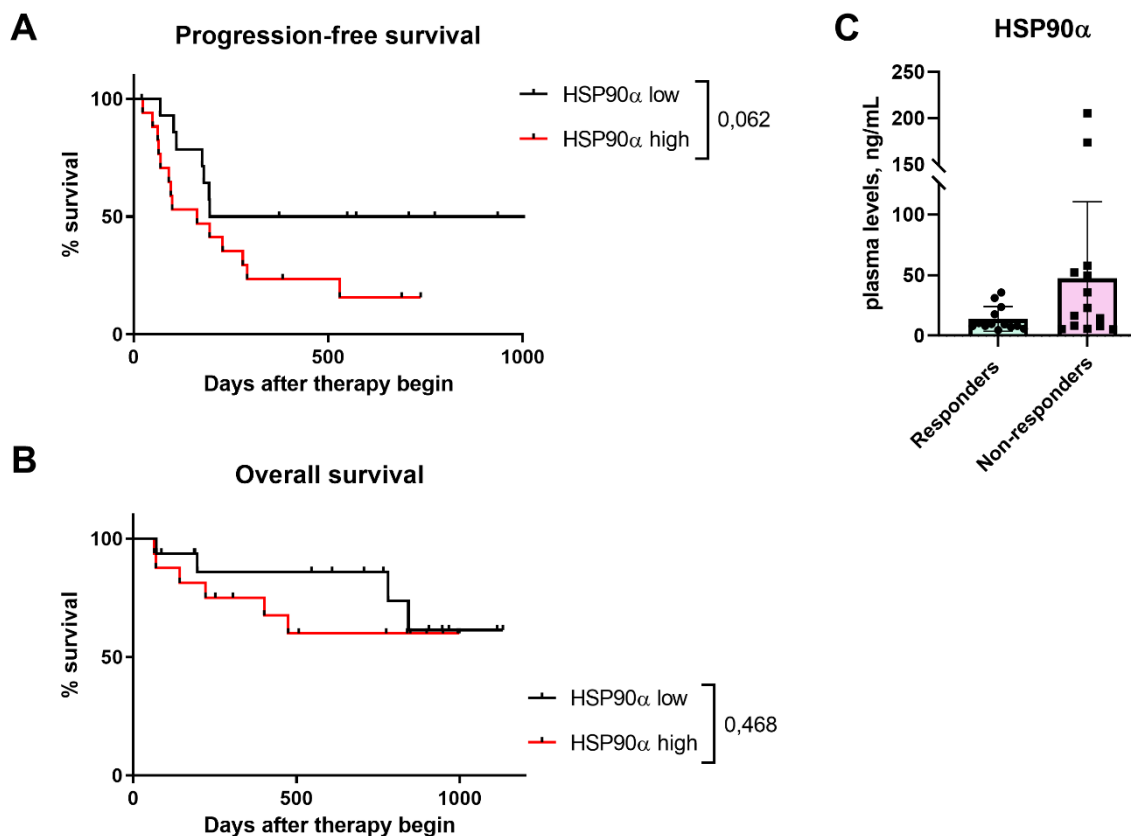


Figure 16. Association between concentration of HSP90 α and clinical outcome of metastatic melanoma patients. The concentration of HSP90 α was measured by ELISA in plasma taken

before the treatment start. **(A)** Progression-free and **(B)** overall survival of melanoma patients with high (>12.42 ng/mL; $n=16$) and low (<12.42 ng/mL; $n=16$) HSP90 α levels at the baseline are shown as a Kaplan-Meier curve. **(C)** The level of HSP90 α in melanoma patients responding ($n=13$) and non-responding ($n=14$) to ICI treatment was expressed in ng/mL (mean \pm SD). ELISA was performed in collaboration with Rebekka Bitsch and Feyza Gul Ozbay Kurt.

6 DISCUSSION

6.1 Control of the LPS contamination in the rHSP90 α

For testing the hypothesis of myeloid cell conversion into MDSC by soluble HSP90 α , we have chosen to stimulate human circulating monocytes isolated from healthy donors buffy coat by rHSP90 α . Since the most likely receptor to interact with HSP90 α on monocytes is TLR4³⁹ we tested the level of contamination by the classical TLR4 ligand LPS, especially due to the fact that most available recombinant proteins are expressed in bacterial systems. Given that proteins denature upon the heating, we tested the activity of several commercially available rHSP90 α expressed in *E. coli* or in insect cells (thought to be LPS-free systems) upon 30 min incubation at 95°C. As a readout, we used upregulation of PD-L1 expression. We have found that almost all preparations, except for the “source 2 lot 1” that was unfortunately no longer available, were LPS-contaminated according to the heat-resistant PD-L1 upregulation. Hence, we established an expression system that would enable us to yield an LPS-free protein using phase separation by Triton X-114¹²¹ combined with the Ni-NTA protein purification method, which enables complete removal of the buffer. Resulting contamination was at least 10 times lower than in commercial preparations, which was not able to upregulate PD-L1 expression on human monocytes. Moreover, our preparation caused heat-sensitive PD-L1 upregulation indicating that the effect was protein-dependent. However, heat-inactivation control of LPS contamination has limitations since Gao et al. showed that the LPS contamination as low as 1 EU/ml can still be heat-sensitive¹²⁴. Therefore, we applied an additional control with trypsin digestion and found that the PD-L1 upregulation effect disappeared after the digestion. Finally, we tested rHSP90 α in the mouse immature myeloid cells and found no upregulation of PD-L1. In contrast, those cells were shown to be activated by LPS³⁹. Altogether, these findings allowed to conclude that the LPS contamination in our rHSP90 α preparation was negligible.

6.2 Upregulation of PD-L1 in rHSP90 α -treated monocytes is TLR4-NF- κ B-dependent

TEV are known to convert myeloid cells into MDSC⁴¹. The complexity of signals carried by TEV demands to dissect the single components of TEV and responsible signaling pathways in recipient cells. It was previously shown that melanoma-derived EV could convert human monocytes into MDSC PD-L1 upregulation mainly via TLR4-signaling³⁹. Other TLRs were also shown to be involved in the PD-L1 upregulation revealing the complexity of EV signals. Importantly, EV isolated from HSP90 α knock-down melanoma cell lines or from melanoma cells treated with the HSP90 α inhibitor (KNK 437) lost their conversion capacity. In the present study, we hypothesized that a single component of melanoma-derived EV, HSP90 α , might be capable to induce conversion of monocytes into MDSC. As a first step, we demonstrated that rHSP90 α could upregulate PD-L1 on human monocytes in a TLR4-dependent manner similarly to melanoma-derived EV. Chen et al. reported that HSP90 α on the surface of tumor cell-released autophagosomes interacted with TLR2 on the surface of CD4⁺ T cells reprogramming them to an immunosuppressive tumor-promoting phenotype¹²⁵. In our experiments on monocytes, anti-TLR2 blocking antibody did not affect the rHSP90 α -mediated upregulation of PD-L1. In order to study the downstream signaling of TLR4, we applied an NF- κ B inhibitor Bay and found that the PD-L1 upregulation was NF- κ B-dependent that was unanimous with the findings of Bohonowych et al. regarding NF- κ B upregulation by eHSP90 α ¹⁰⁵. Since STAT3 activation plays a pivotal role in the generation of MDSC⁶³ we studied an activation of STAT3 and found an NF- κ B-dependent upregulation of STAT3 phosphorylation in monocytes upon the treatment with rHSP90 α . Simultaneous activation of NF- κ B and STAT3 by eHSP90 α is in agreement with the study of Fan et al. in macrophages that found that the mentioned signaling cascades were involved in HSP90 α -mediated macrophage M2-polarisation leading to increased angiogenesis and enhanced tumor growth¹²⁶.

Another receptor reported to interact with HSP90 α is LRP1 (CD91)^{126–128}. Zou et al. found that two evolutionarily conserved lysine residues of HSP90 α , lys-270 and lys-277, expressed in the subfragments F-5 and F-6 were responsible for binding of HSP90 α to LRP1 in cancer cells¹⁰⁷. In our hands, these subfragments, in contrast to full-length HSP90 α , were unable to upregulate PD-L1 in human monocytes that could be due to different effects of this protein on cancer cells and monocytes.

In a recent study, Fan et al. showed that rHSP90 α triggered both LRP1 and TLR4 on THP1-derived macrophages, RAW264.7 macrophage cell line and bone marrow-derived macrophages resulting in upregulation of CD163, CD204, and IL-10, in downregulation of TNF- α , IL-1 β and in depletion of CD4 T cell from the pancreatic tumor¹²⁶. It is possible that HSP90 α in myeloid cells forms a complex with TLR4 and LRP1, in which TLR4 plays a pivotal role. Besides, both α and β isoforms of HSP90 were reported to be present on the surface of monocytes and macrophages and to participate in cytokine response to TLR ligands, building a signaling complex with TLRs including TLR4^{129,130}. The hypothesis of HSP90 α acting as a “signaling complex chaperone”¹²⁹ needs further verification in the context of monocytes conversion into MDSC. Since blocking TLR4 abrogated the upregulation of PD-L1 completely, we concluded that TLR4 is a key receptor for interaction with rHSP90 α that results in the acquisition of immunosuppressive phenotype by monocytes.

Pro-motility effects of eHSP90 α ^{98,107} raised a question whether the stimulation of human monocytes with rHSP90 α would also lead to increased migration capacity. To prove this, we firstly confirmed the pro-motility effect of rHSP90 α in HT144 melanoma cell line in the presence of serum. Next, we tested the migration capacity of rHSP90 α -treated monocytes but found no difference compared to control monocytes. This strengthened the conclusion that eHSP90 α exerts different effects depending on the recipient cells: LRP1-dependent promotility

effect in cancer cells and TLR4-dependent induction of immunosuppressive phenotype in myeloid cells.

6.3 rHSP90 α modifies monocytes towards the suppressive phenotype with prolonged survival

We have shown that rHSP90 α downregulated HLA-DR in monocytes. Low expression of this marker is considered to distinguish human M-MDSC from monocytes²⁵. Frequencies of HLA-DR^{lo/neg} M-MDSC, were shown to be higher in melanoma patients compared to healthy donors^{18,31}. Moreover, M-MDSC levels were higher in patients resistant to the treatment with ipilimumab^{18,31} or nivolumab³⁰. This suggests that neither anti-CTLA-4 nor anti-PD-1 therapy is enough to overcome M-MDSC-mediated immunosuppression and highlights the need for tools to hamper M-MDSC generation.

Investigating the stimulation of monocytes with rHSP90 α was the retention of the monocyte marker CD14 in the stimulated cells compared to the drastic loss of CD14 in the control cells. CD14 receptor is involved in the TLR4 recognition of bacterial cell wall components as well as in the phagocytic clearance of apoptotic cells¹³¹. CD14 downregulation was reported to be caused by IL-2, IL-4, IL-13, IFN- γ ^{132,133}, by histamine via H2-receptors¹³⁴ or by glucocorticoid therapy¹³⁵. Upregulation of CD14 can be induced by DMSO, active 1,25-dihydroxyvitamin D3 [1,25(OH)2D3] and LPS¹³¹. As these reports were not sufficient to explain the retention of CD14 expression in our system we hypothesized it to be related to cell viability and the loss of CD14 to be associated with the undergoing apoptosis. We wanted to precisely measure percentage of cell in the process of apoptosis because the early apoptotic cells are still gated as “live” in our standard assay but can already have altered cell membrane content and possibly lose CD14 expression.

Analysis of monocytes viability was performed by Annexin V and 7-AAD staining and revealed increased viability of rHSP90 α -treated monocytes as the number of AnnexinV⁻7-AAD⁻ cells increased. This finding corresponds to the anti-apoptotic effect of eHSP90 on

monocytic cell line U937 as demonstrated by Franco et al.¹³⁶ Pro-survival effect of rHSP90 α was subsequently shown to be TLR4 but not TLR2 and NF- κ B-dependent that was consistent with above described effects of rHSP90 α . As expected, expression of CD14 was not significantly different among the live (AnnexinV⁻7-AAD⁻) treated and control cells but was strongly downregulated in the early apoptotic cells (AnnexinV⁺7-AAD⁻) regardless of the treatment. Hence, CD14 retaining effect could be explained by higher proportion of live cells among the stimulated monocytes and, in fact, changes in CD14 led us to the discovery of this pro-survival activity of rHSP90 α .

In order to decipher the underlying mechanism of increased survival in rHSP90 α -treated monocytes we tested RNA levels of several pro- and anti-apoptotic genes that are involved in the regulation of survival and death of human monocytes such as caspase 3, BAX, MCL 1, and BCL 2¹³⁷. However, none of the tested genes showed a significant change leaving open the question of how rHSP90 α increases the survival of monocytes.

6.4 Human monocytes acquire PD-L1-mediated suppressive capacity against T cells after stimulation with rHSP90 α

A key feature for defining myeloid cell as “MDSC” is their inhibition of T cell functions²⁶. We have demonstrated that rHSP90 α -treated monocytes inhibit proliferation of CD3 T cells and that their suppressive capacity is abrogated by blocking PD-L1. Noman et al. (2014) have demonstrated that PD-L1 is involved in the inhibition of T cells¹³⁸. However, since non-responders to anti-PD-1 treatment showed high prevalence of M-MDSC³⁰ there is a need for more complex targeting of MDSC. The fact that PD-L1 expression was induced via TLR4-signaling rises an opportunity for inhibiting suppressive activity of rHSP90 α -treated monocytes by inhibiting TLR4 signaling that is known to enhance MDSC activity and was considered as a target for MDSC depletion already some time ago¹³⁹. However, there are contradicting reports showing that TLR4 inhibitor Resatorvid (TAK-242) induces MDSC¹⁴⁰ or that stimulation of

TLR4 by cinnamaldehyde lead to apoptotic death of MDSC¹⁴¹. Apparently, the magnitude, timing and molecular context determine the outcomes of TLR4 signaling. Interestingly, when we added the blocking anti-PD-L1 antibody to the co-culture of rHSP90 α -treated monocytes and T cells, it restored the proliferation not to the same extent as in the co-culture with control monocytes. The involvement of additional suppressive molecules⁴⁷ might have shed light into the residual suppressive activity. We studied whether rHSP90 α influenced the monocyte production of suppressive ROS and NO, the expression of enzymes producing suppressive adenosine (CD39 and CD73) and arginase-1 but found no differences upon rHSP90 α -stimulation of monocytes.

6.5 Microarray analysis of rHSP90 α -treated monocytes identifies upregulation of *IDO1* and several MDSC-related genes

For a comprehensive view on rHSP90 α -mediated effects, we studied transcriptomic changes in rHSP90 α -treated monocytes compared with untreated monocytes. As expected, we confirmed the upregulation of the *CD274*. We have also found an upregulation of genes that are relevant for MDSC recruitment and expansion such as *CCL2*, *CXCL5*, *IL-6*^{36,142} and downregulation of co-stimulatory molecule *CD86*. A monocyte activation marker *CD38* and another co-stimulatory molecule *CD80* were upregulated but less significantly than MDSC-related genes.

An important finding was the upregulation of *IDO1* that was further confirmed at the protein level. *IDO1*⁺ mononuclear cells have been found in melanoma TME, and tumor cell expression of *IDO1* was shown to be positively correlated with PD-L1 expression¹⁴³. Moreover, higher frequencies of *IDO*⁺ M-MDSC were associated with advanced melanoma stage¹⁴⁴. We have shown the functionality of *IDO1* upregulation by the inhibition of T cell proliferation. Combination of anti-CTLA-4, anti-PD-1/PD-L1, and *IDO* inhibition demonstrated a benefit over monotherapy in B16 mouse melanoma model¹⁴⁵. In our experiments, blocking either PD-

L1 or IDO1 alone in rHSP90 α -monocytes restored proliferation of T cells almost up to the basal proliferation level of stimulated T cells cultured alone thus leaving a narrow window for further improvement. Thus, when exploring the synergistic effect of anti-PD-L1 blocking antibody and IDO1 inhibition, we observed no significant difference compared to the monotherapy. However, T cells from two healthy donors showed “response” to one or another treatment approaches, indicating an individual sensitivity. This phenomenon requires further verification.

6.6 Association between concentration of HSP90 α and clinical outcome of patients with metastatic melanoma

In order to verify the clinical significance of our findings on rHSP90 α in melanoma patients, we measured HSP90 α levels in patients’ plasma and investigated the frequency of monocytes and M-MDSC as well as their expression of PD-L1. Since we defined monocytes as CD33⁺HLA-DR^{high} and M-MDSC as CD33⁺HLA-DR^{low}, it was expected to see a tendency of the decrease in monocyte frequencies in patients with higher HSP90 α concentration. This finding goes in line with our *in vitro* data of HLA-DR downregulation in monocytes upon HSP90 α treatment. However, we have not seen a corresponding increase in M-MDSC frequencies (data not shown) that might be explained by an increased migration of M-MDSC into the tumor site. Regarding the PD-L1 expression on circulating M-MDSC, we found a significant positive correlation with higher HSP90 α concentration. Furthermore, we observed a tendency for a worse prognosis among patients expressing higher plasma HSP90 α that goes in line with the literature data¹¹⁴.

6.7 Conclusion

This thesis demonstrates a mechanism of TLR4-NF- κ B-dependent induction of PD-L1⁺IDO1⁺ M-MDSC by HSP90 α (Figure 17). Inhibiting intracellular HSP90 was demonstrated to deplete MDSC^{104,146,147} but none of the available inhibitors of intracellular HSP90 have so

far demonstrated sufficient benefits in clinical trials to be approved for the clinical application. Our study highlights the role of extracellular HSP90 α that might be better target for monotherapy or a combinatorial melanoma treatment. Moreover, we have showed prognostic and predictive value of plasma levels of HSP90 α in melanoma patients that goes in line with literature findings on HSP90 α in cancer^{112–114}.

Main results of the present work were published in Arkhypov I, Özbay Kurt FG, Bitsch R, Novak D, Petrova V, Lasser S, et al. HSP90 α induces immunosuppressive myeloid cells in melanoma via TLR4 signaling. *J Immunother Cancer*. 2022;10(9):e005551. doi:10.1136/jitc-2022-005551/01.09.2022.

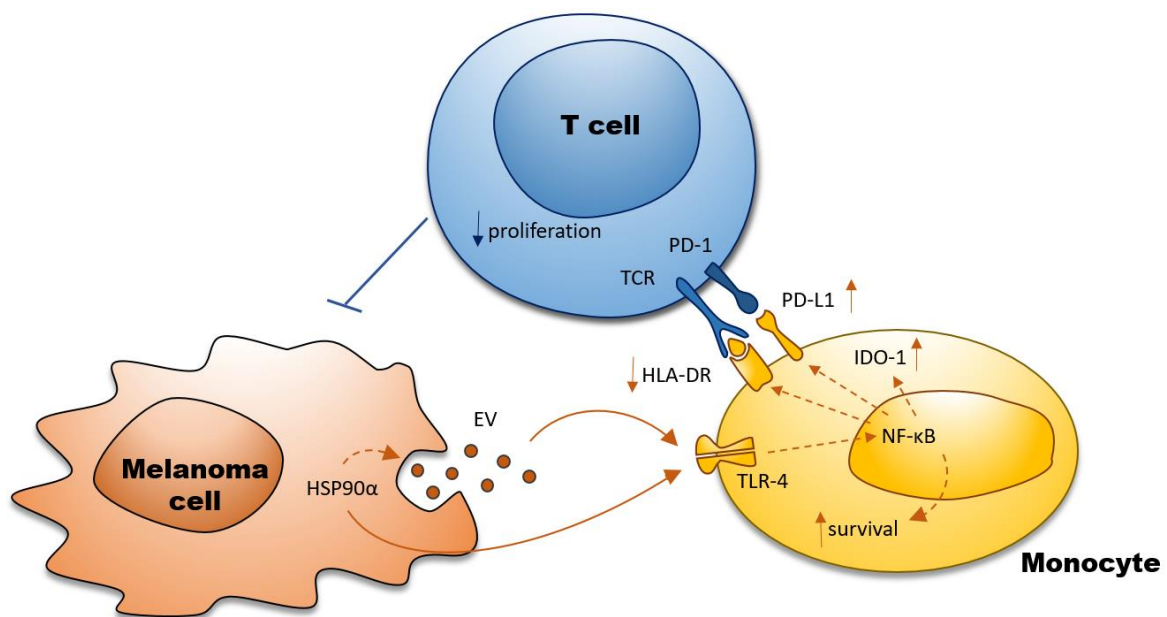


Figure 14. HSP90 α induces immunosuppressive myeloid cells in melanoma via TLR4 signaling. HSP90 α can be secreted by melanoma cells in association with EV or as a soluble protein. Soluble HSP90 α can trigger TLR4-NF- κ B cascade, leading to upregulation of PD-L1, IDO-1, downregulation of HLA-DR and prolonged survival of monocytes. Altogether these features endow monocytes with suppressive activity against T cells.

7 REFERENCES

1. Eggermont AMM, Spatz A, Robert C: Cutaneous melanoma. *Lancet*, 383:816-827, 2014. doi: 10.1016/S0140-6736(13)60802-8.
2. Michielin O, van Akkooi ACJ, Ascierto PA, Dummer R, Keilholz U: Cutaneous melanoma: ESMO Clinical Practice Guidelines for diagnosis, treatment and follow-up. *Ann Oncol*, 30:1884-1901, 2019. doi: 10.1093/annonc/mdz411
3. Amaria RN, Menzies AM, Burton EM, Scolyer RA, Tetzlaff MT, Antdbacka R, et al.: Neoadjuvant systemic therapy in melanoma: recommendations of the International Neoadjuvant Melanoma Consortium. *Lancet Oncol*, 20:e378-e389, 2019. doi: 10.1016/S1470-2045(19)30332-8.
4. Bommareddy PK, Patel A, Hossain S, Kaufman HL: Talimogene Laherparepvec (T-VEC) and Other Oncolytic Viruses for the Treatment of Melanoma. *Am J Clin Dermatol*, 18: 1-15, 2017. doi: 10.1007/s40257-016-0238-9.
5. Kozar I, Margue C, Rothengatter S, Haan C, Kreis S: Many ways to resistance: How melanoma cells evade targeted therapies. *Biochim Biophys Acta Rev Cancer*, 1871: 313-322, 2019. doi: 10.1016/j.bbcan.2019.02.002
6. Petrova V, Arkhypov I, Weber R, Groth C, Altevogt P, Utikal J, et al.: Modern Aspects of Immunotherapy with Checkpoint Inhibitors in Melanoma. *Int J Mol Sci*, 21:2367, 2020. doi: 10.3390/ijms21072367
7. Passarelli A, Mannavola F, Stucci LS, Tucci M, Silvestris F: Immune system and melanoma biology: a balance between immunosurveillance and immune escape. *Oncotarget*, 8: 106132-106142, 2017. doi: 10.18632/oncotarget.22190
8. Simiczyjew A, Dratkiewicz E, Mazurkiewicz J, Ziętek M, Matkowski R, Nowak D: The Influence of Tumor Microenvironment on Immune Escape of Melanoma. *Int J Mol Sci*, 21: 8359, 2020. doi: 10.3390/ijms21218359
9. Marzagalli M, Ebel ND, Manuel ER: Unraveling the crosstalk between melanoma and immune cells in the tumor microenvironment. *Semin Cancer Biol*, 59: 236–250, 2019. doi: 10.1016/j.semcancer.2019.08.002
10. Rodig SJ, Gusenleitner D, Jackson DG, Gjini E, Giobbie-Hurder A, Jin C, et al.: MHC proteins confer differential sensitivity to CTLA-4 and PD-1 blockade in untreated metastatic melanoma. *Sci Transl Med*, 10: eaar3342, 2018. doi: 10.1126/scitranslmed.aa3342
11. Poggio M, Hu T, Pai CC, Chu B, Belair CD, Chang A, et al.: Suppression of Exosomal PD-L1 Induces Systemic Anti-tumor Immunity and Memory. *Cell*, 177: :414-427.e13, 2019. doi: 10.1016/j.cell.2019.02.016
12. Yu C, Liu X, Yang J, Zhang M, Jin H, Ma X, et al.: Combination of immunotherapy with targeted therapy: Theory and practice in metastatic melanoma. *Front Immunol*, 10:990, 2019. doi: 10.3389/fimmu.2019.00990

13. Rauschenberg R, Bruns J, Brütting J, Daubner D, Lohaus F, Zimmer L, et al.: Impact of radiation, systemic therapy and treatment sequencing on survival of patients with melanoma brain metastases. *Eur J Cancer* 110: 11-20, 2019. doi: 10.1016/j.ejca.2018.12.023
14. Afzal MZ, Mercado RR, Shirai K: Efficacy of metformin in combination with immune checkpoint inhibitors (anti-PD-1/anti-CTLA-4) in metastatic malignant melanoma. *J Immunother Cancer* 6: 64, 2018. doi: 10.1186/s40425-018-0375-1
15. Ribas A, Dummer R, Puzanov I, VanderWalde A, Andtbacka RHI, Michielin O, et al.: Oncolytic Virotherapy Promotes Intratumoral T Cell Infiltration and Improves Anti-PD-1 Immunotherapy. *Cell*, 170: 1109-1119, 2017. doi: 10.1016/j.cell.2017.08.027
16. Krebs FK, Trzeciak ER, Zimmer S, Özistanbullu D, Mitzel-Rink H, Meissner M, et al.: Immune signature as predictive marker for response to checkpoint inhibitor immunotherapy and overall survival in melanoma. *Cancer Med*, 10: 1562–1575, 2021. doi: 10.1002/cam4.3710
17. Jordan KR, Amaria RN, Ramirez O, Callihan EB, Gao D, Borakove M, et al.: Myeloid-derived suppressor cells are associated with disease progression and decreased overall survival in advanced-stage melanoma patients. *Cancer Immunol Immunother*, 62: 1711–1722, 2013. doi: 10.1007/s00262-013-1475-x
18. Meyer C, Cagnon L, Costa-Nunes CM, Baumgaertner P, Montandon N, Leyvraz L, et al.: Frequencies of circulating MDSC correlate with clinical outcome of melanoma patients treated with ipilimumab. *Cancer Immunol Immunother*, 63: 247–257, 2014. doi: 10.1007/s00262-013-1508-5
19. Wong PF, Wei W, Gupta S, Smithy JW, Zeltermann D, Kluger HM, et al.: Multiplex quantitative analysis of cancer-associated fibroblasts and immunotherapy outcome in metastatic melanoma. *J Immunother Cancer*, 7: 194, 2019. doi: 10.1186/s40425-019-0675-0
20. Moses K, Brandau S: Human neutrophils: Their role in cancer and relation to myeloid-derived suppressor cells. *Semin Immunol*, 28: 187-196, 2016. doi: 10.1016/j.smim.2016.03.018
21. Xie X, Liu J, Yang H, Chen H, Zhou S, Lin H, et al.: Prognostic Value of Baseline Neutrophil-to-Lymphocyte Ratio in Outcome of Immune Checkpoint Inhibitors. *Cancer Invest*, 37: 265-274, 2019. doi: 10.1080/07357907.2019.1639057
22. Zhang Y, Liu G, Sun M, Lu X: Targeting and exploitation of tumor-associated neutrophils to enhance immunotherapy and drug delivery for cancer treatment. *Cancer Biol Med*, 17: 32-43, 2020. doi: 10.20892/j.issn.2095-3941.2019.0372
23. Eggermont AM, Ascierto PA, Khushalani NI, Schadendorf D, Boland G, Weber J, et al.: PIVOT-12: a phase III study of adjuvant bimepegaldesleukin plus nivolumab in resected stage III/IV melanoma at high risk for recurrence. *Future Oncol*, 18: 903-913, 2022. doi: 10.2217/fon-2021-1286
24. Etzerodt A, Tsalkitzi K, Maniecki M, Damsky W, Delfini M, Baudoin E, et al.: Specific targeting of CD163 + TAMs mobilizes inflammatory monocytes and promotes T cell-mediated tumor regression. *J Exp Med*, 216: 2394–2411, 2019. doi: 10.1084/jem.20182124

25. Veglia F, Perego M, Gabrilovich D: Myeloid-derived suppressor cells coming of age review-article. *Nat Immunol*, 19: 108–119, 2018. doi: 10.1038/s41590-017-0022-x
26. Bronte V, Brandau S, Chen SH, Colombo MP, Frey AB, Greten TF, et al.: Recommendations for myeloid-derived suppressor cell nomenclature and characterization standards. *Nat Commun*, 7: 12150, 2016. doi: 10.1038/ncomms12150
27. Condamine T, Dominguez GA, Youn JI, Kossenkova A v., Mony S, Alicea-Torres K, et al.: Lectin-type oxidized LDL receptor-1 distinguishes population of human polymorphonuclear myeloid-derived suppressor cells in cancer patients. *Sci Immunol*, 1: aaf8943, 2016. doi: 10.1126/sciimmunol.aaf8943
28. Huber V, di Guardo L, Lalli L, Giardiello D, Cova A, Squarcina P, et al.: Back to simplicity: a four-marker blood cell score to quantify prognostically relevant myeloid cells in melanoma patients. *J Immunother Cancer*, 9: e001167, 2021. doi: 10.1136/jitc-2020-001167
29. Jiang H, Gebhardt C, Umansky L, Beckhove P, Schulze TJ, Utikal J, et al.: Elevated chronic inflammatory factors and myeloid-derived suppressor cells indicate poor prognosis in advanced melanoma patients. *Int J Cancer*, 136: 2352–2360, 2015. doi: 10.1002/ijc.29297
30. Weber J, Gibney G, Kudchadkar R, Yu B, Cheng P, Martinez AJ, et al.: Phase I/II Study of Metastatic Melanoma Patients Treated with Nivolumab Who Had Progressed after Ipilimumab. *Cancer Immunol Res*, 4: 345–353, 2016. doi: 10.1158/2326-6066.CIR-15-0193
31. Gebhardt C, Sevko A, Jiang H, Lichtenberger R, Reith M, Tarnanidis K, et al.: Myeloid Cells and Related Chronic Inflammatory Factors as Novel Predictive Markers in Melanoma Treatment with Ipilimumab. *Clin Cancer Res*, 21: 5453–5459, 2015. doi: 10.1158/1078-0432.CCR-15-0676
32. Heinemann AS, Pirr S, Fehlhaber B, Mellinger L, Burgmann J, Busse M, et al.: In neonates S100A8/S100A9 alarmins prevent the expansion of a specific inflammatory monocyte population promoting septic shock. *FASEB J*, 31: 1153–1164, 2017. doi: 10.1096/fj.201601083R
33. Mach N, Gillessen S, Wilson SB, Sheehan C, Mihm M, Dranoff G: Differences in dendritic cells stimulated in vivo by tumors engineered to secrete granulocyte-macrophage colony-stimulating factor or Flt3-ligand. *Cancer Res*, 60: 3239–3246, 2000.
34. Condamine T, Gabrilovich DI: Molecular mechanisms regulating myeloid-derived suppressor cell differentiation and function. *Trends Immunol*, 32: 19–25, 2011. doi: 10.1016/j.it.2010.10.002
35. Bayne LJ, Beatty GL, Jhala N, Clark CE, Rhim AD, Stanger BZ, et al.: Tumor-derived granulocyte-macrophage colony-stimulating factor regulates myeloid inflammation and T cell immunity in pancreatic cancer. *Cancer Cell*, 21: 822–835, 2012. doi: 10.1016/j.ccr.2012.04.025
36. Weber R, Groth C, Lasser S, Arkhypov I, Petrova V, Altevogt P, et al.: IL-6 as a major regulator of MDSC activity and possible target for cancer immunotherapy. *Cell Immunol*, 359: 104254, 2021. doi: 10.1016/j.cellimm.2020.104254

37. Mastio J, Condamine T, Dominguez G, Kossenkova A v., Donthireddy L, Veglia F, et al.: Identification of monocyte-like precursors of granulocytes in cancer as a mechanism for accumulation of PMN-MDSCs. *J Exp Med*, 216: 2150–2169, 2019. doi: 10.1084/jem.20181952
38. Huber V, Vallacchi V, Fleming V, Hu X, Cova A, Dugo M, et al.: Tumor-derived microRNAs induce myeloid suppressor cells and predict immunotherapy resistance in melanoma. *J Clin Invest*, 128: 5505–5516, 2018. doi: 10.1172/JCI98060
39. Fleming V, Hu X, Weller C, Weber R, Groth C, Riester Z, et al.: Melanoma Extracellular Vesicles Generate Immunosuppressive Myeloid Cells by Upregulating PD-L1 via TLR4 Signaling. *Cancer Res*, 79: 4715–4728, 2019. doi: 10.1158/0008-5472.CAN-19-0053
40. Mao Y, Poschke I, Wennerberg E, de Coaña YP, Brage SE, Schultz I, et al.: Melanoma-educated CD14+ cells acquire a myeloid-derived suppressor cell phenotype through COX-2-dependent mechanisms. *Cancer Res*, 73: 3877–3887, 2013. doi: 10.1158/0008-5472.CAN-12-4115
41. Arkhypov I, Lasser S, Petrova V, Weber R, Groth C, Utikal J, et al.: Myeloid Cell Modulation by Tumor-Derived Extracellular Vesicles. *Int J Mol Sci*, 21: 6319, 2020. doi: 10.3390/ijms21176319
42. Chang AL, Miska J, Wainwright DA, Dey M, Rivetta C v., Yu D, et al.: CCL2 Produced by the Glioma Microenvironment Is Essential for the Recruitment of Regulatory T Cells and Myeloid-Derived Suppressor Cells. *Cancer Res*, 76: 5671–5682, 2016. doi: 10.1158/0008-5472.CAN-16-0144
43. Cheng Y, Ma X lei, Wei Y quan, Wei XW: Potential roles and targeted therapy of the CXCLs/CXCR2 axis in cancer and inflammatory diseases. *Biochim Biophys Acta Rev Cancer*, 1871: 289–312, 2019. doi: 10.1016/j.bbcan.2019.01.005
44. Groth C, Arpinati L, Shaul ME, Winkler N, Diester K, Gengenbacher N, et al.: Blocking Migration of Polymorphonuclear Myeloid-Derived Suppressor Cells Inhibits Mouse Melanoma Progression. *Cancers (Basel)*, 13: 726, 2021. doi: 10.3390/cancers13040726
45. Weber R, Riester Z, Hüser L, Sticht C, Siebenmorgen A, Groth C, et al.: IL-6 regulates CCR5 expression and immunosuppressive capacity of MDSC in murine melanoma. *J Immunother Cancer*, 8: e000949, 2020. doi: 10.1136/jitc-2020-000949
46. Blattner C, Fleming V, Weber R, Himmelhan B, Altevogt P, Gebhardt C, et al.: CCR5 + Myeloid-Derived Suppressor Cells Are Enriched and Activated in Melanoma Lesions. *Cancer Res*, 78: 157–167, 2018. doi: 10.1158/0008-5472.CAN-17-0348
47. Groth C, Hu X, Weber R, Fleming V, Altevogt P, Utikal J, et al.: Immunosuppression mediated by myeloid-derived suppressor cells (MDSCs) during tumour progression. *Br J Cancer*, 120: 16–25, 2019. doi: 10.1038/s41416-018-0333-1
48. Yu J, Du W, Yan F, Wang Y, Li H, Cao S, et al.: Myeloid-derived suppressor cells suppress antitumor immune responses through IDO expression and correlate with lymph node metastasis in patients with breast cancer. *J Immunol*, 190: 3783–3797, 2013. doi: 10.4049/jimmunol.1201449

49. Fleming V, Hu X, Weber R, Nagibin V, Groth C, Altevogt P, et al.: Targeting Myeloid-Derived Suppressor Cells to Bypass Tumor-Induced Immunosuppression. *Front Immunol*, 9: 398, 2018. doi: 10.3389/fimmu.2018.00398
50. Mirza N, Fishman M, Fricke I, Dunn M, Neuger AM, Frost TJ, et al.: All-trans-retinoic acid improves differentiation of myeloid cells and immune response in cancer patients. *Cancer Res*, 66: 9299-9307, 2006. doi: 10.1158/0008-5472.CAN-06-1690
51. Nefedova Y, Fishman M, Sherman S, Wang X, Beg AA, Gabrilovich DI: Mechanism of all-trans retinoic acid effect on tumor-associated myeloid-derived suppressor cells. *Cancer Res*, 67: 11021-11028, 2007. doi: 10.1158/0008-5472.CAN-07-2593
52. Iclozan C, Antonia S, Chiappori A, Chen DT, Gabrilovich D: Therapeutic regulation of myeloid-derived suppressor cells and immune response to cancer vaccine in patients with extensive stage small cell lung cancer. *Cancer Immunol Immunother*, 62: 909-918, 2013. doi: 10.1007/s00262-013-1396-8
53. Michels T, Shurin G v., Naiditch H, Sevko A, Umansky V, Shurin MR: Paclitaxel promotes differentiation of myeloid-derived suppressor cells into dendritic cells in vitro in a TLR4-independent manner. *J Immunotoxicol*, 9: 292-300, 2012. doi: 10.3109/1547691X.2011.642418
54. Sevko A, Michels T, Vrohling M, Umansky L, Beckhove P, Kato M, et al.: Antitumor Effect of Paclitaxel Is Mediated by Inhibition of Myeloid-Derived Suppressor Cells and Chronic Inflammation in the Spontaneous Melanoma Model. *J Immunol*, 190: 2464-2471, 2013. doi: 10.4049/jimmunol.1202781
55. Serafini P, Meckel K, Kelso M, Noonan K, Califano J, Koch W, et al.: Phosphodiesterase-5 inhibition augments endogenous antitumor immunity by reducing myeloid-derived suppressor cell function. *J Exp Med*, 203: 2691-2702, 2006. doi: 10.1084/jem.20061104
56. Lin S, Wang J, Wang L, Wen J, Guo Y, Qiao W, et al.: Phosphodiesterase-5 inhibition suppresses colonic inflammation-induced tumorigenesis via blocking the recruitment of MDSC. *Am J Cancer Res*, 7: 41-52, 2017.
57. Meyer C, Sevko A, Ramacher M, Bazhin A v., Falk CS, Osen W, et al.: Chronic inflammation promotes myeloid-derived suppressor cell activation blocking antitumor immunity in transgenic mouse melanoma model. *Proc Natl Acad Sci U S A* 108: 17111- 17116, 2011. doi: 10.1073/pnas.1108121108
58. Weed DT, Vella JL, Reis IM, de La Fuente AC, Gomez C, Sargi Z, et al.: Tadalafil reduces myeloid-derived suppressor cells and regulatory t cells and promotes tumor immunity in patients with head and neck squamous cell carcinoma. *Clin Cancer Res* 21: 39-48, 2015. doi: 10.1158/1078-0432.CCR-14-1711
59. Hassel JC, Jiang H, Bender C, Winkler J, Sevko A, Shevchenko I, et al.: Tadalafil has biologic activity in human melanoma. Results of a pilot trial with Tadalafil in patients with metastatic Melanoma (TaMe). *Oncoimmunology*, 6: e1326440, 2017. doi: 10.1080/2162402X.2017.1326440

60. Califano JA, Khan Z, Noonan KA, Rudraraju L, Zhang Z, Wang H, et al.: Tadalafil augments tumor specific immunity in patients with head and neck squamous cell carcinoma. *Clin Cancer Res*, 21: 30-38, 2015. doi: 10.1158/1078-0432.CCR-14-1716
61. Kim K, Skora AD, Li Z, Liu Q, Tam AJ, Blosser RL, et al.: Eradication of metastatic mouse cancers resistant to immune checkpoint blockade by suppression of myeloid-derived cells. *Proc Natl Acad Sci U S A* 111: 11774-11779, 2014. doi: 10.1073/pnas.1410626111
62. Orillion A, Hashimoto A, Damayanti N, Shen L, Adelaiye-Ogala R, Arisa S, et al.: Entinostat neutralizes myeloid-derived suppressor cells and enhances the antitumor effect of PD-1 inhibition in murine models of lung and renal cell carcinoma. *Clin Cancer Res*, 23: 5187-5201, 2017. doi: 10.1158/1078-0432.CCR-17-0741
63. Bitsch R, Kurzay A, Özbay Kurt F, de La Torre C, Lasser S, Lepper A, et al.: STAT3 inhibitor Napabucasin abrogates MDSC immunosuppressive capacity and prolongs survival of melanoma-bearing mice. *J Immunother Cancer*, 10: e004384, 2022. doi: 10.1136/jitc-2021-004384
64. van Niel G, D'Angelo G, Raposo G: Shedding light on the cell biology of extracellular vesicles. *Nat Rev Mol Cell Biol*, 19: 213-228, 2018. doi: 10.1038/nrm.2017.125
65. Shi S, Rao Q, Zhang C, Zhang X, Qin Y, Niu Z: Dendritic Cells Pulsed with Exosomes in Combination with PD-1 Antibody Increase the Efficacy of Sorafenib in Hepatocellular Carcinoma Model. *Transl Oncol*, 11: 250–258, 2018. doi: 10.1016/j.tranon.2018.01.001
66. Asadirad A, Hashemi SM, Baghaei K, Ghanbarian H, Mortaz E, Zali MR, et al.: Phenotypical and functional evaluation of dendritic cells after exosomal delivery of miRNA-155. *Life Sci*, 219: 152-162, 2019. doi: 10.1016/j.lfs.2019.01.005
67. Taghikhani A, Hassan ZM, Ebrahimi M, Moazzeni SM: microRNA modified tumor-derived exosomes as novel tools for maturation of dendritic cells. *J Cell Physiol*, 234: 9417-9427, 2019. doi: 10.1002/jcp.27626
68. Yang C, Kim SH, Bianco NR, Robbins PD: Tumor-derived exosomes confer antigen-specific immunosuppression in a murine delayed-type hypersensitivity model. *PLoS One*, 6: e22517, 2011. doi: 10.1371/journal.pone.0022517
69. Ning Y, Shen K, Wu Q, Sun X, Bai Y, Xie Y, et al.: Tumor exosomes block dendritic cells maturation to decrease the T cell immune response. *Immunol Lett*, 199: 36-43, 2018. doi: 10.1016/j.imlet.2018.05.002
70. Liu J, Fan L, Yu H, Zhang J, He Y, Feng D, et al.: Endoplasmic Reticulum Stress Causes Liver Cancer Cells to Release Exosomal miR-23a-3p and Up-regulate Programmed Death Ligand 1 Expression in Macrophages. *Hepatology*, 70: 241-258, 2019. doi: 10.1002/hep.30607
71. Yin C, Han Q, Xu D, Zheng B, Zhao X, Zhang J: SALL4-mediated upregulation of exosomal miR-146a-5p drives T-cell exhaustion by M2 tumor-associated macrophages in HCC. *Oncoimmunology*, 8: 1601479, 2019. doi: 10.1080/2162402X.2019.1601479

72. Ying X, Wu Q, Wu X, Zhu Q, Wang X, Jiang L, et al.: Epithelial ovarian cancer-secreted exosomal miR-222-3p induces polarization of tumor-associated macrophages. *Oncotarget*, 7: 43076-43087, 2016. doi: 10.18632/oncotarget.9246
73. Qian M, Wang S, Guo X, Wang J, Zhang Z, Qiu W, et al.: Hypoxic glioma-derived exosomes deliver microRNA-1246 to induce M2 macrophage polarization by targeting TERF2IP via the STAT3 and NF- κ B pathways. *Oncogene*, 39: 428–442, 2020. doi: 10.1038/s41388-019-0996-y
74. Park JE, Dutta B, Tse SW, Gupta N, Tan CF, Low JK, et al.: Hypoxia-induced tumor exosomes promote M2-like macrophage polarization of infiltrating myeloid cells and microRNA-mediated metabolic shift. *Oncogene* 38: 5158-5173, 2019. doi: 10.1038/s41388-019-0782-x
75. Ren WH, Zhang XR, Li WB, Feng Q, Feng HJ, Tong Y, et al.: Exosomal miRNA-107 induces myeloid-derived suppressor cell expansion in gastric cancer. *Cancer Manag Res*, 11: 4023-4040, 2019. doi: 10.2147/CMAR.S198886
76. Bruns H, Böttcher M, Qorraj M, Fabri M, Jitschin S, Dindorf J, et al.: CLL-cell-mediated MDSC induction by exosomal miR-155 transfer is disrupted by Vitamin D. *Leukemia*, 31:985-988, 2017. doi: 10.1038/leu.2016.378
77. Guo X, Qiu W, Wang J, Liu Q, Qian M, Wang S, et al.: Glioma exosomes mediate the expansion and function of myeloid-derived suppressor cells through microRNA-29a/Hbp1 and microRNA-92a/Prkar1a pathways. *Int J Cancer*, 144: 3111-3126, 2019. doi: 10.1002/ijc.32052
78. Guo X, Qiu W, Liu Q, Qian M, Wang S, Zhang Z, et al.: Immunosuppressive effects of hypoxia-induced glioma exosomes through myeloid-derived suppressor cells via the miR-10a/Rora and miR-21/Pten Pathways. *Oncogene*, 37: 4239-4259, 2018. doi: 10.1038/s41388-018-0261-9
79. Li L, Cao B, Liang X, Lu S, Luo H, Wang Z, et al.: Microenvironmental oxygen pressure orchestrates an anti- and pro-tumoral $\gamma\delta$ T cell equilibrium via tumor-derived exosomes. *Oncogene*, 38: 2830-2843, 2019. doi: 10.1038/s41388-018-0627-z
80. Xiang X, Liu Y, Zhuang X, Zhang S, Michalek S, Taylor DD, et al.: TLR2-mediated expansion of MDSCs is dependent on the source of tumor exosomes. *Am J Pathol*, 177: 1606-1610, 2010. doi: 10.2353/ajpath.2010.100245
81. Chalmin F, Ladoire S, Mignot G, Vincent J, Bruchard M, Remy-Martin JP, et al.: Membrane-associated Hsp72 from tumor-derived exosomes mediates STAT3-dependent immunosuppressive function of mouse and human myeloid-derived suppressor cells. *J Clin Invest*, 120: 457-471, 2010. doi: 10.1172/JCI40483
82. Gobbo J, Marcion G, Cordonnier M, Dias AMM, Pernet N, Hammann A, et al.: Restoring Anticancer Immune Response by Targeting Tumor-Derived Exosomes with a HSP70 Peptide Aptamer. *J Natl Cancer Inst*, 108: 2016. doi: 10.1093/jnci/djv330
83. Diao J, Yang X, Song X, Chen S, He Y, Wang Q, et al.: Exosomal Hsp70 mediates immunosuppressive activity of the myeloid-derived suppressor cells via phosphorylation of Stat3. *Med Oncol*, 32: 453, 2015. doi: 10.1007/s12032-014-0453-2

84. Yu S, Liu C, Su K, Wang J, Liu Y, Zhang L, et al.: Tumor Exosomes Inhibit Differentiation of Bone Marrow Dendritic Cells. *J Immunology*, 178: 6867-6875, 2007. doi: 10.4049/jimmunol.178.11.6867
85. Pyzer AR, Stroopinsky D, Rajabi H, Washington A, Tagde A, Coll M, et al.: MUC1-mediated induction of myeloid-derived suppressor cells in patients with acute myeloid leukemia. *Blood*, 129: 1791-1801, 2017. doi: 10.1182/blood-2016-07-730614
86. Plebanek MP, Angeloni NL, Vinokour E, Li J, Henkin A, Martinez-Marin D, et al.: Pre-metastatic cancer exosomes induce immune surveillance by patrolling monocytes at the metastatic niche. *Nat Commun*, 8: 1319, 2017. doi: 10.1038/s41467-017-01433-3
87. Wang F, Li B, Wei Y, Zhao Y, Wang L, Zhang P, et al.: Tumor-derived exosomes induce PD1+ macrophage population in human gastric cancer that promotes disease progression. *Oncogenesis*, 7: 41, 2018. doi: 10.1038/s41389-018-0049-3
88. Valenti R, Huber V, Filipazzi P, Pilla L, Sovena G, Villa A, et al.: Human tumor-released microvesicles promote the differentiation of myeloid cells with transforming growth factor- β -mediated suppressive activity on T lymphocytes. *Cancer Res*, 66: 9290-9298, 2006. doi: 10.1158/0008-5472.CAN-06-1819
89. Gabrusiewicz K, Li X, Wei J, Hashimoto Y, Marisetty AL, Ott M, et al.: Glioblastoma stem cell-derived exosomes induce M2 macrophages and PD-L1 expression on human monocytes. *Oncoimmunology*, 7: e1412909, 2018. doi: 10.1080/2162402X.2017.1412909
90. Iorgulescu JB, Ivan ME, Safaee M, Parsa AT: The limited capacity of malignant glioma-derived exosomes to suppress peripheral immune effectors. *J Neuroimmunol*, 290: 103-108, 2016. doi: 10.1016/j.jneuroim.2015.11.025
91. Javeed N, Gustafson MP, Dutta SK, Lin Y, Bamlet WR, Oberg AL, et al.: Immunosuppressive CD14+HLA-DRlo/neg monocytes are elevated in pancreatic cancer and “primed” by tumor-derived exosomes. *Oncoimmunology*, 6: e1252013, 2017. doi: 10.1080/2162402X.2016.1252013
92. Birbo B, Madu EE, Madu CO, Jain A, Lu Y: Role of HSP90 in Cancer. *Int J Mol Sci*, 22: 10317, 2021. doi: 10.3390/ijms221910317
93. Schopf FH, Biebl MM, Buchner J: The HSP90 chaperone machinery. *Nat Rev Mol Cell Biol*, 18: 345–360, 2017. doi: 10.1038/nrm.2017.20
94. Seo YH: Organelle-specific Hsp90 inhibitors. *Arch Pharm Res*, 38: 1582–1590, 2015. doi: 10.1007/s12272-015-0636-1
95. Li W, Sahu D, Tsen F: Secreted heat shock protein-90 (Hsp90) in wound healing and cancer. *Biochim Biophys Acta*, 1823: 730–741, 2012. doi: 10.1016/j.bbamcr.2011.09.009
96. Becker B, Multhoff G, Farkas B, Wild PJ, Landthaler M, Stolz W, et al.: Induction of Hsp90 protein expression in malignant melanomas and melanoma metastases. *Exp Dermatol*, 13: 27–32, 2004. doi: 10.1111/j.0906-6705.2004.00114.x

97. Barrott JJ, Haystead TAJ: Hsp90, an unlikely ally in the war on cancer. *FEBS J*, 280: 1381–1396, 2013. doi: 10.1111/febs.12147
98. Daniel Jay, Yongzhang Luo, Wei Li: Extracellular Heat Shock Protein-90 (eHsp90): Everything You Need to Know. *Biomolecules*, 12: 911, 2022. doi: 10.3390/biom12070911
99. Dvorak HF: Tumors: Wounds that do not heal-redux. *Cancer Immunol Res*, 3: 1-11, 2015. doi: 10.1158/2326-6066.CIR-14-020
100. Dvorak HF: Tumors: Wounds That Do Not Heal. *N Engl J Med*, 315: 1650-1659, 1986. doi: 10.1056/NEJM198612253152606
101. Haggerty TJ, Dunn IS, Rose LB, Newton EE, Pandolfi F, Kurnick JT: Heat shock protein-90 inhibitors enhance antigen expression on melanomas and increase T cell recognition of tumor cells. *PLoS One*, 9: e114506, 2014. doi: 10.1371/journal.pone.0114506
102. Joshi SS, Jiang S, Unni E, Goding SR, Fan T, Antony PA, et al.: 17-AAG inhibits vemurafenib-associated MAP kinase activation and is synergistic with cellular immunotherapy in a murine melanoma model. *PLoS One*, 13: e0191264, 2018. doi: 10.1371/journal.pone.0191264
103. Mbofung RM, McKenzie JA, Malu S, Zhang M, Peng W, Liu C, et al.: HSP90 inhibition enhances cancer immunotherapy by upregulating interferon response genes. *Nat Commun*, 8: 451, 2017. doi: 10.1038/s41467-017-00449-z
104. Janssen N, Speigl L, Pawelec G, Niessner H, Shipp C: Inhibiting HSP90 prevents the induction of myeloid-derived suppressor cells by melanoma cells. *Cell Immunol*, 327: 68–76, 2018. doi: 10.1016/j.cellimm.2018.02.012
105. Bohonowych JE, Hance MW, Nolan KD, Defee M, Parsons CH, Isaacs JS: Extracellular Hsp90 mediates an NF- κ B dependent inflammatory stromal program: implications for the prostate tumor microenvironment. *Prostate*, 74: 395–407, 2014. doi: 10.1002/pros.22761
106. McCready J, Sims JD, Chan D, Jay DG: Secretion of extracellular hsp90alpha via exosomes increases cancer cell motility: a role for plasminogen activation. *BMC Cancer*, 10: 294, 2010. doi: 10.1186/1471-2407-10-294
107. Zou M, Bhatia A, Dong H, Jayaprakash P, Guo J, Sahu D, et al.: Evolutionarily conserved dual lysine motif determines the non-chaperone function of secreted Hsp90alpha in tumour progression. *Oncogene*, 36: 2160–2171, 2017. doi: 10.1038/onc.2016.375
108. Wang X, Song X, Zhuo W, Fu Y, Shi H, Liang Y, et al.: The regulatory mechanism of Hsp90 secretion and its function in tumor malignancy. *Proc Natl Acad Sci U S A*, 106: 21288–21293, 2009. doi: 10.1073/pnas.0908151106
109. Tian Y, Wang C, Chen S, Liu J, Fu Y, Luo Y: Extracellular Hsp90 α and clusterin synergistically promote breast cancer epithelial-to-mesenchymal transition and metastasis via LRP1. *J Cell Sci*, 132: jcs228213, 2019. doi: 10.1242/jcs.228213
110. Zhang S, Wang C, Ma B, Xu M, Xu S, Liu J, et al.: Mutant p53 Drives Cancer Metastasis via RCP-Mediated Hsp90 α Secretion. *Cell Rep*, 32: 107879, 2020. doi: 10.1016/j.celrep.2020.107879

111. Hou Q, Chen S, An Q, Li B, Fu Y, Luo Y: Extracellular hsp90 α promotes tumor lymphangiogenesis and lymph node metastasis in breast cancer. *Int J Mol Sci*, 22: 7747, 2021. doi: 10.3390/ijms22147747
112. Liu W, Li J, Zhang P, Hou Q, Feng S, Liu L, et al.: A novel pan-cancer biomarker plasma heat shock protein 90 α and its diagnosis determinants in clinic. *Cancer Sci*, 110: 2941–2959, 2019. doi: 10.1111/cas.14143
113. Chen S, Yu Q, Zhou S: Plasmatic Levels of HSP90 α at Diagnosis: A Novel Prognostic Indicator of Clinical Outcome in Advanced Lung Cancer Patients Treated With PD-1/PD-L1 Inhibitors Plus Chemotherapy. *Front Oncol*, 11: 765115, 2021. doi: 10.3389/fonc.2021.765115
114. Zhang T, Li Q, Zhang Y, Wang Q, Wang H, Gu K: Diagnostic and prognostic value of heat shock protein 90 α in malignant melanoma. *Melanoma Res*, 31: 152–161, 2021. doi: 10.1097/CMR.0000000000000716
115. Smyth GK: Linear models and empirical bayes methods for assessing differential expression in microarray experiments. *Stat Appl Genet Mol Biol*, 3: Article3, 2004. doi: 10.2202/1544-6115.1027
116. Smyth GK: limma: Linear Models for Microarray Data. In: *Bioinformatics and Computational Biology Solutions Using R and Bioconductor*, Springer, New York, 2005, p. 397–420. doi.org/10.1007/0-387-29362-0_23
117. Wu D, Smyth GK: Camera: a competitive gene set test accounting for inter-gene correlation. *Nucleic Acids Res* 40: e133, 2012. doi: 10.1093/nar/gks461
118. Kanehisa M, Goto S: KEGG: kyoto encyclopedia of genes and genomes. *Nucleic Acids Res*, 28: 27–30, 2000. doi: 10.1093/nar/28.1.27
119. Fabregat A, Jupe S, Matthews L, Sidiropoulos K, Gillespie M, Garapati P, et al.: The Reactome Pathway Knowledgebase. *Nucleic Acids Res*, 46: D649–D655, 2018. doi: 10.1093/nar/gkx1132
120. Bordier C: Phase separation of integral membrane proteins in Triton X-114 solution. *Journal of Biological Chemistry* 256: 1604-1607, 1981.
121. Aida Y, Pabst MJ: Removal of endotoxin from protein solutions by phase separation using Triton X-114. *J Immunol Methods*, 132: 191–195, 1990. doi: 10.1016/0022-1759(90)90029-u
122. Cassetta L, Bruderek K, Skrzeczynska-Moncznik J, Osiecka O, Hu X, Rundgren IM, et al.: Differential expansion of circulating human MDSC subsets in patients with cancer, infection and inflammation. *J Immunother Cancer*, 8: e001223, 2020. doi: 10.1136/jitc-2020-001223
123. Hudig D, Hunter KW, Diamond WJ, Redelman D: Properties of human blood monocytes. I. CD91 expression and log orthogonal light scatter provide a robust method to identify monocytes that is more accurate than CD14 expression. *Cytometry B Clin Cytom* 86: 111-120, 2014. doi: 10.1002/cyto.b.21131
124. Gao B, Wang Y, Tsan M-F: The heat sensitivity of cytokine-inducing effect of lipopolysaccharide. *J Leukoc Biol*, 80: 359–366, 2006. doi: 10.1189/jlb.1205738

125. Chen YQ, Li PC, Pan N, Gao R, Wen ZF, Zhang TY, et al.: Tumor-released autophagosomes induces CD4 + T cell-mediated immunosuppression via a TLR2-IL-6 cascade. *J Immunother Cancer*, 7: 178, 2019. doi: 10.1186/s40425-019-0646-5
126. Fan CS, Chen CC, Chen LL, Chua KV, Hung HC, Hsu JTA, et al.: Extracellular HSP90 α Induces MyD88-IRAK Complex-Associated IKK α / β -NF- κ B/IRF3 and JAK2/TYK2-STAT-3 Signaling in Macrophages for Tumor-Promoting M2-Polarization. *Cells*, 11: 229, 2022. doi: 10.3390/cells11020229
127. Ding X, Meng C, Dong H, Zhang S, Zhou H, Tan W, et al.: Extracellular Hsp90 α , which participates in vascular inflammation, is a novel serum predictor of atherosclerosis in type 2 diabetes. *BMJ Open Diabetes Res Care*, 10: e002579, 2022. doi: 10.1136/bmjdr-2021-002579
128. Dong H, Luo L, Zou M, Huang C, Wan X, Hu Y, et al.: Blockade of extracellular heat shock protein 90 α by 1G6-D7 attenuates pulmonary fibrosis through inhibiting ERK signaling. *Am J Physiol Lung Cell Mol Physiol*, 313: L1006–L1015, 2017. doi: 10.1152/ajplung.00489.2016
129. Bzowska M, Nogiec A, Bania K, Zygmunt M, Zarębski M, Dobrucki J, et al.: Involvement of cell surface 90 kDa heat shock protein (HSP90) in pattern recognition by human monocyte-derived macrophages. *J Leukoc Biol*, 102: 763–774, 2017. doi: 10.1189/jlb.2MA0117-019R
130. Cecchini P, Tavano R, Polverino de Laureto P, Franzoso S, Mazzon C, Montanari P, et al.: The soluble recombinant *Neisseria meningitidis* adhesin NadA(Δ 351-405) stimulates human monocytes by binding to extracellular Hsp90. *PLoS One*, 6: e25089, 2011. doi: 10.1371/journal.pone.0025089
131. Zamani F, Shahneh FZ, Aghebati-Maleki L, Baradaran B: Induction of CD14 Expression and Differentiation to Monocytes or Mature Macrophages in Promyelocytic Cell Lines: New Approach. *Adv Pharm Bull*, 3: 329-332, 2013. doi: 10.5681/apb.2013.053
132. Viale G, Vercelli D: Interleukin-13 regulates the phenotype and function of human monocytes. *Int Arch Allergy Immunol*, 107: 176–178, 1995. doi: 10.1159/000236969
133. Landmann R, Ludwig C, Obrist R, Obrecht JP: Effect of cytokines and lipopolysaccharide on CD14 antigen expression in human monocytes and macrophages. *J Cell Biochem*, 47: 317–329, 1991. doi: 10.1159/000236969
134. Takahashi HK, Morichika T, Iwagaki H, Tamura R, Kubo S, Yoshino T, et al.: Histamine downregulates CD14 expression via H2 receptors on human monocytes. *Clin Immunol*, 108: 274–281, 2003. doi: 10.1016/s1521-6616(03)00140-2
135. Sümegi A, Antal-Szalmás P, Aleksza M, Kovács I, Sipka S, Zeher M, et al.: Glucocorticosteroid therapy decreases CD14-expression and CD14-mediated LPS-binding and activation of monocytes in patients suffering from systemic lupus erythematosus. *Clin Immunol*, 117: 271–279, 2005. doi: 10.1016/j.clim.2005.09.002
136. Franco L, Terrinca J, Rodríguez AB, Espino J, Pariente JA: Extracellular heat shock proteins protect U937 cells from H₂O₂-induced apoptotic cell death. *Mol Cell Biochem*, 412: 19–26, 2016. doi: 10.1007/s11010-015-2604-y

137. Parihar A, Eubank TD, Doseff AI: Monocytes and macrophages regulate immunity through dynamic networks of survival and cell death. *J Innate Immun*, 2: 204-215, 204–215, 2010. doi: 10.1159/000296507
138. Noman MZ, Desantis G, Janji B, Hasmim M, Karray S, Dessen P, et al.: PD-L1 is a novel direct target of HIF-1 α , and its blockade under hypoxia enhanced MDSC-mediated T cell activation. *J Exp Med*, 211: 781–790, 2014. doi: 10.1084/jem.20131916
139. Bunt SK, Clements VK, Hanson EM, Sinha P, Ostrand-Rosenberg S: Inflammation enhances myeloid-derived suppressor cell cross-talk by signaling through Toll-like receptor 4. *J Leukoc Biol*, 85: 996–1004, 2009. doi: 10.1189/jlb.0708446
140. Wang H, Li X, Dong G, Yan F, Zhang J, Shi H, et al.: Toll-like Receptor 4 Inhibitor TAK-242 Improves Fulminant Hepatitis by Regulating Accumulation of Myeloid-Derived Suppressor Cell. *Inflammation*, 44: 671–681, 2021. doi: 10.1007/s10753-020-01366-y
141. He W, Zhang W, Zheng Q, Wei Z, Wang Y, Hu M, et al.: Cinnamaldehyde causes apoptosis of myeloid-derived suppressor cells through the activation of TLR4. *Oncol Lett*, 18: 2420–2426, 2019. doi: 10.3892/ol.2019.10544
142. Kumar V, Patel S, Tcyganov E, Gabrilovich DI: The nature of myeloid-derived suppressor cells in the tumor microenvironment. *Trends Immunol*, 37: 208-220, 2016. doi: 10.1016/j.it.2016.01.004
143. Gide TN, Allanson BM, Menzies AM, Ferguson PM, Madore J, Saw RPM, et al.: Inter- and inpatient heterogeneity of indoleamine 2,3-dioxygenase expression in primary and metastatic melanoma cells and the tumour microenvironment. *Histopathology*, 74: 817–828, 2019. doi: 10.1111/his.13814
144. Chevolet I, Speeckaert R, Schreuer M, Neyns B, Krysko O, Bachert C, et al.: Characterization of the in vivo immune network of IDO, tryptophan metabolism, PD-L1, and CTLA-4 in circulating immune cells in melanoma. *Oncoimmunology*, 4: e982382, 2015. doi: 10.4161/2162402X.2014.982382
145. Spranger S, Koblish HK, Horton B, Scherle PA, Newton R, Gajewski TF: Mechanism of tumor rejection with doublets of CTLA-4, PD-1/PD-L1, or IDO blockade involves restored IL-2 production and proliferation of CD8(+) T cells directly within the tumor microenvironment. *J Immunother Cancer*, 2: 3, 2014. doi: 10.1186/2051-1426-2-3
146. Rao A, Taylor JL, Chi-Sabins N, Kawabe M, Gooding WE, Storkus WJ: Combination therapy with HSP90 inhibitor 17-DMAG reconditions the tumor microenvironment to improve recruitment of therapeutic T cells. *Cancer Res*, 72: 3196–3206, 2012. doi: 10.1158/0008-5472.CAN-12-0538
147. Liu Y, Qiu N, Shen L, Liu Q, Zhang J, Cheng YY, et al.: Nanocarrier-mediated immunogenic chemotherapy for triple negative breast cancer. *J Control Release*, 323: 431–441, 2020. doi: 10.1016/j.jconrel.2020.04.040

8 CURRICULUM VITAE

PERSONAL DATA:

Name and Surname: Ihor Arkhypov
 Date of birth: 27.06.1995
 Place of birth: Dnipro, Ukraine
 Marital status: Single

SCHOOL EDUCATION:

2002-2009 Primary and middle school (Dnipro, Ukraine)
 2009-2012 Medical lyceum “Dnipro” (Dnipro, Ukraine)
 06/2012 “Attestat” (German – “Abitur”)

UNIVERSITY EDUCATION:

09/2012-06/2018 Human medicine at O.O. Bogomolets National Medical University, Kiev, Ukraine. Graduated with honors
 Since 02/2019 Doctoral student at Medizinische Fakultät Mannheim der Universität Heidelberg
 08/2020-07/2021 Residency (ukr. „Internatura“, ger. „Assistenzarzt“) in pathology at O.O. Bogomolets National Medical University, Kiev, Ukraine

PROFESSIONAL CAREER:

08/2018-02/2019 assistant tutor at Pathophysiology department, O.O. Bogomolets National Medical University, Kiev, Ukraine

9 LIST OF OWN PUBLICATIONS DURING THE THESIS WORK

Arkhypov I*, Özbay Kurt FG*, Bitsch R, Novak D, Petrova V, Lasser S, Hielscher T, Groth C, Lepper A, Hu X, Li W, Utikal J, Altevogt P, Umansky V. HSP90 α induces immunosuppressive myeloid cells in melanoma via TLR4 signaling. *J Immunother Cancer*. 2022 Sep;10(9):e005551. doi: 10.1136/jitc-2022-005551 (*equally contributed)

Groth C, Arpinati L, Shaul ME, Winkler N, Diester K, Gengenbacher N, Weber R, **Arkhypov I**, Lasser S, Petrova V, Augustin HG, Altevogt P, Utikal J, Fridlender ZG, Umansky V. Blocking Migration of Polymorphonuclear Myeloid-Derived Suppressor Cells Inhibits Mouse Melanoma Progression. *Cancers (Basel)*. 2021 Feb 10;13(4):726. doi: 10.3390/cancers13040726

Hüser L, Kokkaleniou MM, Granados K, Dworacek J, Federico A, Vierthaler M, Novak D, **Arkhypov I**, Hielscher T, Umansky V, Altevogt P, Utikal J. HER3-Receptor-Mediated STAT3 Activation Plays a Central Role in Adaptive Resistance toward Vemurafenib in Melanoma. *Cancers (Basel)*. 2020 Dec 14;12(12):3761. doi: 10.3390/cancers12123761

Weber R, Groth C, Lasser S, **Arkhypov I**, Petrova V, Altevogt P, Utikal J, Umansky V. IL-6 as a major regulator of MDSC activity and possible target for cancer immunotherapy. *Cell Immunol*. 2021 Jan;359:104254. doi: 10.1016/j.cellimm.2020.104254

Arkhypov I*, Lasser S*, Petrova V, Weber R, Groth C, Utikal J, Altevogt P, Umansky V. Myeloid Cell Modulation by Tumor-Derived Extracellular Vesicles. *Int J Mol Sci*. 2020 Aug 31;21(17):6319. doi: 10.3390/ijms21176319 (*equally contributed)

Petrova V, **Arkhypov I**, Weber R, Groth C, Altevogt P, Utikal J, Umansky V. Modern Aspects of Immunotherapy with Checkpoint Inhibitors in Melanoma. *Int J Mol Sci*. 2020 Mar 30;21(7):2367. doi: 10.3390/ijms21072367. PMID: 32235439; PMCID: PMC7178114.

10 ACKNOWLEDGEMENTS

Support and commitment of many people and several institutions made this thesis come to light.

My deepest gratitude goes to Prof. Viktor Umansky. Dear Viktor, owing to your wish for spreading scientific knowledge in Ukraine back in 2016 I got an opportunity to work on this thesis. And owing to your patient guidance, attentive surveillance, and wise recommendations the present work is now written. I appreciate a lot your strategic view on the project as well as the attention in all small details when I needed help. Moreover, you patronized me during this time and opened plenty of doors.

Invaluable contribution has been done by Prof. Peter Altevogt. Dear Peter, your energy and motivation are literally contagious. By initiating a necessary pivot at the beginning and by establishing essential collaborations you pushed the work forward and made it fruitful.

Professional guidance through the clinical aspects of the work and the great administrative support I owe to Prof. Jochen Utikal. Insightful feedback during our department meetings from you and from members of your group made the work better.

An integration of a medical student in research life is always challenging. Knowing this by herself, Xiaoying Hu made more than possible to teach me all the necessary methods, settle on the project, and made my start in the lab painless and smooth.

Great help during my start and onward I got from Rebekka Bitsch and Christopher Groth. Your discipline, Rebekka, and your optimization skills, Christopher, demonstrated me the way at work. And your family achievements demonstrated me the way in life.

The accomplishment of the most difficult experiments I owe to Feyza Gül Özbay Kurt. Your perseverance far outweighs all technical problems and the oriental flavor you brought to our lab made every day bright.

Modern science cannot be imagined without proper reagents. Providing the recombinant protein Daniel Novak settled a fundament for the project and I appreciate this contribution a lot, Daniel.

My special joy I owe to my “Doktorschwestern” Vera, Samantha, Feyza, and Alisa. Your friendly words and the warmth spread made me feel happy and helped to manage the obstacles encountering during this time. Working together in the lab would be a pleasure for everyone on my place.

I would like to acknowledge the contribution of Thomas Hielscher for the microarray analysis, Stefanie Uhlig for cell sorting, Yvonne Nowak, Sayran Arif-Said, Vera Petrova, Rebekka Bitsch and Feyza Gül Özbay Kurt for collection of plasma samples.

A further acknowledge is dedicated to our collaboration partner from University of Southern California, Los Angeles, USA, Prof. Wei Li for providing us the HSP90 α plasmid.

Big gratefulness is to Graduate School 2099 „Hallmarks of Skin Cancer“, the head Prof. Sergij Goerd, every single member of the Graduate School, and especially to Martina Nolte-Bohres for all her organizational efforts and personal commitment. Particularly good memories about Summer schools in London will accompany me in the future.

All colleagues from the House 42 and especially Camela Jost together with the library team including Maurizio Grilli, and co-workers from canteen created the proper milieu for the present research.

My parents and my brother Alexander deserve more than gratitude. Although being far away you are still close. You fill me with your love and give the sense of the solid ground during every earthquake. Your advices come faster than I ask and your support stretches beyond the steps I take.

I thank God for meeting all these wonderful people and for putting me in this place in this time.